

Self-similar orbit-averaged Fokker-Planck equation for isotropic spherical dense clusters (iii) application of pre-collapse solution to Galactic globular clusters

Yuta Ito^{a,b}

^a*Department of Physics, CUNY Graduate Center, [☆]*

^b*Department of Engineering and Physics, CUNY College of Staten Island^{☆☆}*

Abstract

This is the third paper of a series of our works on the self-similar orbit-averaged Fokker-Planck (OAFP) equation. The first paper provided an accurate spectral solution of the equation for isotropic pre-collapse star clusters and the second detailed the physical feature of the model. Based on the works, the present work applies the solution to the observed structural profiles of Galactic globular clusters. For fitting to the profiles, the most fundamental (quasi-)stationary model, the King model, and the variants have shown successful results while they can not apply to core-collapsing and core-collapsed clusters at the late stage of the relaxation evolution. We propose an energy-truncated self-similar OAFP model that can apply to clusters at both the early and late stages of the evolution. This new model fits the structural profiles of at least half of Galactic globular clusters while it also applies to core-collapsed stars with resolved cores. As a main result, we provide the completion rate of core collapse against concentration for the clusters. Also, we show our new model can apply to the globular clusters even in a broad range of radii (0.01~10 arcminutes). However, since our model includes polytrope (elongated outer halo), the tidal radius of the model becomes unrealistically large for some clusters. To avoid the issue, we also propose an approximated form of the new model. Lastly, we report that Milky Way globular clusters with low concentrations have the same spatial structures as stellar polytropes and discuss whether such polytropic cluster is a reasonable concept.

Keywords: dense star cluster; core collapse; self-similar evolution; orbit-averaged Fokker-Planck model; isotropic; energy-truncation; Galactic globular clusters; polytrope; post-core-collapsed clusters

1. Introduction

This is the third paper of a series of our works on the self-similar orbit-averaged Fokker-Planck (OAFP) equation for isotropic dense star clusters in pre-collapse phase. The first paper (Ito, 2020a) showed an accurate Gauss-Chebyshev spectral solution of the equation and the second (Ito, 2020b) detailed the physical feature of the model focusing on the negative heat capacity of the core of the model. Based on their results, the present paper proposes a phenomenological model that reasonably fits to the projected structural profiles of Galactic globular clusters that include not only normal (King model) clusters but also core-collapsed (or core-collapsing) clusters with resolved cores. In the rest of the present section, we review the applicability of the most fundamental fitting model (the King model (King, 1966)) to Galactic globular clusters (Section 1.1) and also time-dependent OAFP model (Section 1.2) together with explaining the reason why the pre-collapse solution can even apply to post-collapsed clusters (Section 1.3).

1.1. Applicability of King model to Galactic globular clusters

The most fundamental fitting model for the structures of globular clusters is the King model (King, 1965) that can reasonably apply to globular clusters that are *not* in the late stage of relaxation evolution. Fitting of the King model

[☆]365 Fifth Avenue, New York, NY 10016, USA

^{☆☆}2800 Victory Boulevard, Staten Island, NY 10314, USA

Email address: yito@gradcenter.cuny.edu (Yuta Ito)

depends on the three numerical parameters; the central projected density Σ_c (or surface brightness (SB)), core radius r_c and dimensionless central potential $K(= \varphi(r=0)/\sigma_c)$ where the central potential $\varphi(r=0)$ is normalized by the central velocity dispersion σ_c . Only with the three degrees of freedom, the King model well fits the surface brightness or projected density for approximately 80% of globular clusters in Milky Way; the rest of 20% is considered to be on the verge of core collapse or have undergone core collapse at least once (Djorgovski and King, 1986). In this sense, the clusters that can be fitted by the King model is sometimes called 'normal' or 'King-model' (KM) clusters and those that can not is 'post-collapsed-core' or 'post-core-collapse' (PCC) clusters. The difference between the KM- and PCC- clusters are that (i) the projected structural profile of a typical KM cluster flattens in the core while a typical PCC cluster has a cusp with a power law approximately r^{-1} and (ii) the concentrations of PCC clusters are high $c \gtrsim 2.0$ while those of KM clusters are low $0.7 \lesssim c \lesssim 1.8$ (See e.g. Meylan and Heggie, 1997). The high concentration and cusp are considered as the signatures of post core collapse in the late stage of relaxation evolution.

1.2. Applicability of OAFP- and other models to PCC clusters

The structural profiles of PCC clusters may be fitted by time-dependent OAFP models for spherical clusters in post core-collapsed phase with realistic effects though, alternative models have been developed for homogeneous survey. It is not generally a easy task to self-consistently solve a time-dependent OAFP equation coupled to Poisson equation. As application, a time-dependent OAFP model applies to a certain globular cluster as a case study to discuss its detail structure e.g. (Murphy et al., 2011) for NGC 7088, (Drukier et al., 1992) for NGC 6838 and (Drukier, 1995) for NGC 6397. On one hand, the King model is based only on Poisson equation easy to be solved for the potential of a spherical cluster and it is rather used in homogeneous survey to capture the common properties (the characteristic size of clusters and dynamical states) of as many globular clusters as possible by neglecting the detail information of each cluster. In fact, the concentration, core- and tidal- radii obtained from the King model have been the fundamental structural parameters in compilation works for globular-cluster studies (e.g. Peterson and King, 1975; Trager et al., 1995; Miocchi et al., 2013; Merafina, 2017) and in (Harris, 1996, (2010 edition))'s catalog. To the best of our knowledge, up to date, there does not exist a single-mass isotropic model only based on Poisson equation that applies to both PCC- and KM- clusters due to their different core structures. For PCC clusters, a modified power-law profile (e.g. Lugger et al., 1995; Ferraro et al., 2003) or non-parametric model (e.g. Noyola and Gebhardt, 2006) has been employed in place of the single-component King model, its variants (e.g. Woolley, 1961; Wilson, 1975) and generalized models (e.g. Gomez-Leyton and Velazquez, 2014; Gieles and Zocchi, 2015)¹. The present work focuses on a single-mass model for simplicity though, a multi-mass King model is known to be able to fit some PCC cluster (King et al., 1995) and there is no a strict argument that rules out such multi-mass King model from a proper model for PCC clusters (Meylan and Heggie, 1997).

1.3. Relation of the ss-OAFP model with PCC clusters

Due to its more proper description for the relaxation evolution of star clusters, we expect the ss-OAFP model can well model the structure of globular clusters in the center and inner halo at core-collapsing phase, compared to the King model. Not only this, but also we expect the structure of the ss-OAFP model is similar to those of PCC cluster under certain conditions, which motivated us to apply the ss-OAFP model to cluster structures.

The ss-OAFP model for pre-collapse clusters may be able to fit even the projected structural profiles of PCC clusters due to the structural similarities between pre-collapse- and post-collapse- clusters. In principle, the ss-OAFP model in pre-collapse phase is the model that applies only to globular clusters at the moment of complete core collapse (with infinite central density) and approximately collapsing-core clusters in the late stage of relaxation evolution before the core completely collapses. Also, the ss-OAFP model itself is unrealistic in the sense that binaries halt the collapse in the core before the infinite density develops; the core can have a high density that is enough to form binaries from single stars. After the core collapse holds, time-dependent- and self-similar- conducting gaseous models predict that clusters successively repeat core expansion (due to the energy release from binaries) and core collapse (due to the two body relaxation with self-gravity) (Sugimoto and Bettwieser, 1983; Bettwieser and Sugimoto, 1984;

¹In addition to those generalization, some more recent models can readily integrate into our model, hence we do not discuss the detail relation of our model to those models. e.g. we do not consider the relation of our model to collisionless relaxation based on f_v model (de Vita et al., 2016) and the effect of escapers to discuss the elongated outer halos of some clusters (Claydon et al., 2019).

Goodman, 1984, 1987). This process is called ‘gravothermal oscillation’ in post core-collapse phase since it shows a nonlinear oscillation of core density with time. Time-dependent OAFP models (Cohn et al., 1989; Murphy et al., 1990; Takahashi, 1996) and N -body simulations (Makino, 1996; Breen and Heggie, 2012) also predict the oscillation. Sugimoto and Bettwieser (1983); Bettwieser and Sugimoto (1984) found that the velocity dispersion seems approach the singular isothermal sphere in the outer halo while the core structure is alike the (non-singular) isothermal sphere (except at the moment of core collapse) against the result of the self-similar gaseous model with a central cusp (Inagaki and Lynden-Bell, 1983). The latter seems proper to describe PCC clusters reported in (e.g. Djorgovski and King, 1986) though, formation of a cusp in the core is a conditional result. The self-similar gaseous model of Goodman (1984) showed that the core radius gets smaller with increasing N , which induces a cluster to be overstable or unstable and the cluster undergoes a gravothermal oscillation *if* the cluster has enough stars in it ($N \gtrsim 7 \times 10^3$) as shown by Goodman (1987) based on the same model but with different functional forms of energy source or more efficient binary heating. The Goodman (1984)’s model results in forming a cusp in the core while Goodman (1987)’s model has a core like a non-singular isothermal sphere. In fact, to avoid unrealistically small- and large- core, efficient binary heating with primordial binaries is expected to occur, which still can form possibly resolved cores (Goodman and Hut, 1989). In addition, the structural profile with a resolved core in the post-collapse phase of the gaseous model (Goodman, 1987) and OAFP model (Takahashi, 1996) are similar to the profiles for the corresponding pre-collapse core. There is no way to differentiate the structural profiles in the two phases only from observational data (Meylan and Heggie, 1997) unless one acquires accurate kinematic data to see the temperature inversion². This infers that some PCC clusters with efficient binary heating may be modeled by the ss-OAFP model. This is a motivation to apply the (core-collapsing) ss-OAFP model to PCC clusters and the present purpose of our new model is, of course, to find structural parameters of PCC clusters with resolved core rather than establishing strict modeling of them.

The present paper proposes an energy-truncated ss-OAFP model that can fit the structural profiles of Galactic KM- and PCC- clusters *with resolved cores* reported in (Kron et al., 1984; Djorgovski and King, 1986; Trager et al., 1995; Lugger et al., 1995; Drukier et al., 1993; Ferraro et al., 2003; Noyola and Gebhardt, 2006; Miocchi et al., 2013). Since we did not have access to the data of (Djorgovski and King, 1986; Lugger et al., 1995; Miocchi et al., 2013), we employed *WebPlotDigitizer* (Rohatgi, 2019) to extract data points and their uncertainties for the projected density and surface brightness profiles depicted on figures of their works. The present paper is organized as follows. Section 2 introduces the energy truncated ss-OAFP model to be fitted to the projected structural profiles of Galactic globular clusters. Section 3 explains the result of fitting the new model to PCC clusters. Section 4 shows the relationship between the completion rate of core collapse and concentration based on the results of the fitting of our model to KM- and PCC- clusters. Section 5 discusses application of our model with higher index m to globular clusters in a broad range of radii, proposes the approximated form of the new model and suggests that low-concentration globular clusters may have structures described by stellar polytropes (or polytropic spheres) of index m . Section 6 concludes the paper. For the sake of brevity, in Appendixes A, B and C, we show the majority of the projected density profiles and surface brightness fitted by the energy-truncated ss-OAFP model.

2. Energy-truncated ss-OAFP model

The present section introduces an energy-truncated ss-OAFP model. First, Section 2.1 shows the relation of the ss-OAFP model to the isothermal sphere with a motivation for truncating energy of the ss-OAFP model. Section 2.2 details the new model. The new model does not depend on dimensionless central potential K , hence Section 2.3 explains how to regularize the concentration and core radius of the new model to compare the new model to the King model. Also, our model is composed of a polytrope of m and the ss-OAFP model and we must choose the value of m for our model, hence Section 2.4 explains how we found an optimal value of m .

²A distinct difference between the OAFP models in core-collapsing and core-collapsed phases appears in the radial profile for velocity dispersion (Sugimoto and Bettwieser, 1983). When the core-collapsed core expands, the temperature (velocity dispersion) increases with radius near the center of cluster, which causes heat to flow inward toward the center and cools down the center. Kinematic survey, however, in general provides much larger uncertainty in velocity dispersion compared to structural data (Meylan and Heggie, 1997). Hence, one can not easily determine if a well-relaxed (or high-concentration) cluster is currently in pre-collapse- or post-collapse- phases.

2.1. Relation of the ss-OAFP model with the isothermal sphere

The ss-OAFP model can model KM clusters since the model has flat (quasi-)isothermal core that can be directly inferred from our numerical result of (Ito, 2020b). There exists a similar structure in the cores between the ss-OAFP model and the isothermal sphere model as discussed in (Ito, 2020b) for the local properties. The ss-OAFP model has almost the same morphology in density profile as that of the isothermal sphere as shown in Figure 1. In the figure, the radius of the ss-OAFP model is rescaled by multiplying by 3.739 so that the core size of the two models is approximately the same. This core structure infers that by properly truncating energy of the ss-OAFP model one may also obtain a model similar to the King model at small radii; we explain how to truncate the energy in Section 2.2.

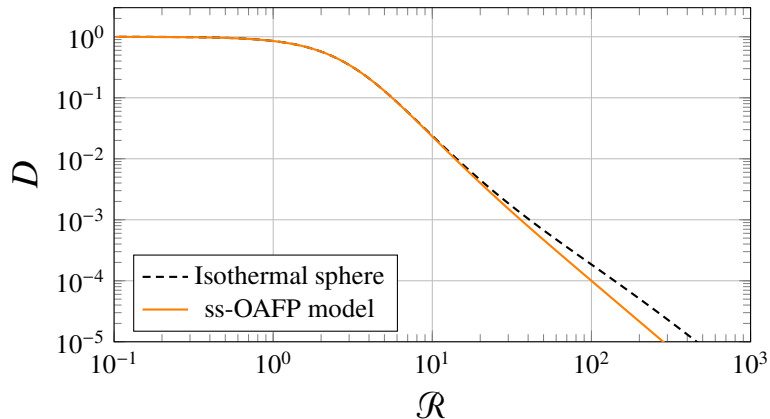


Figure 1: Dimensionless densities $D(\mathcal{R})$ of the isothermal sphere and ss-OAFP model.

2.2. Energy-truncated ss-OAFP model

We energy-truncate the ss-OAFP model by considering the outer halo of our new model behaves like a polytrope of m , hence the model is to a *phenomenological* model unlike the King model (King, 1966). The energy truncation of the King model is based on relatively-simple physical models and arguments using ‘test particle’ method assuming particles (stars) other than the test particle (star) follow Maxwellian DF e.g. the King model may be a star cluster described by stationary FP model (Spitzer and Harm, 1958; Michie, 1962; King, 1965) and OAFP model (Spitzer and Shapiro, 1972) of isothermal sphere enclosed in a square well, and the stellar DF proportional to $-E$ is an asymptotic stationary solution of the OAFP model with constant stellar flux at the fringe (Spitzer and Shapiro, 1972)³. Our new model incorporates the effect of the escaping stars in a similar way to (King, 1966) by controlling high binding energy, but the mathematical operation for combining DF is opposite to King (1966)’s method. To obtain the King model (or lowered-Maxwellian DF), one must subtract DF for polytrope of $m = 2.5$ from Maxwellian DF. On one hand, our energy-truncated ss-OAFP model adds DF for a polytrope of m to the reference DF $F_o(E)$ for the ss-OAFP model (found in (Ito, 2020a) as follows

$$\tilde{F}(E) \equiv \frac{\rho_c}{4\sqrt{2}\pi\sigma_c^3} \frac{F_o(E) + \delta(-E)^{m-3/2}}{D_o(\varphi = -1) + \delta B(m - 1/2, 3/2)}, \quad (2.1)$$

where δ and m are positive real numbers, $D_o(\varphi)$ is the reference density for the ss-OAFP model (found in (Ito, 2020a) and $B(a, b)$ is the beta function defined as $B(a, b) = 2 \int_0^1 t^{2a-1}(1-t^2)^{b-1} dt$ with $a > 1/2$ and $b > 1$. The factor $1/(D_o(\varphi = -1) + \delta B(m - 1/2, 3/2))$ is inserted in the DF so that the density profile for the DF $\tilde{F}(E)$ has a certain central density ρ_c as $R \rightarrow 0$. This new DF behaves like the ss-OAFP model beyond order of δ in equation (2.1) while below δ it is approximately a polytropic sphere of index m . Yet, the value of m must be further fixed⁴ based

³The stellar DF proportional $-E$ is the higher-energy limit of the lowered-Maxwellian DF.

⁴Since the index m in our model is to be determined at first place, our model has the same parameter-dependence as the truncated γ exponential (fractional-power) model proposed in (Gomez-Leyton and Velazquez, 2014) in the sense that the outer halo is controlled by a polytropic sphere.

on physical arguments (with numerical experiments) and from observational data. In this work, we do only the latter process (Section 2.4). In this sense, we consider our model a phenomenological model.

The rest of the present section shows numerically calculated density profile, m.f. potential and projected density profile for the energy-truncated ss-OAFP model. One can analytically derive the explicit form of the density profile for polytropes, hence the density for our new truncated model reads

$$D(\varphi) = \rho_c \frac{D_o(\varphi) + \delta B(m - 1/2, 3/2) (-\varphi)^m}{D_o(\varphi = -1) + \delta B(m - 1/2, 3/2)}. \quad (2.2)$$

Poisson equation for potential $\varphi(r)$ of an isotropic spherical cluster reads

$$\frac{d^2\varphi}{dr^2} + \frac{2}{r} \frac{d\varphi}{dr} = \rho[\varphi(r)] \equiv 16\pi^2 G D(\varphi). \quad (2.3)$$

where G is the gravitational constant. The dimensionless form of the Poisson equation reads

$$\frac{d^2\bar{\varphi}}{d\bar{r}^2} + \frac{2}{\bar{r}} \frac{d\bar{\varphi}}{d\bar{r}} = \bar{\rho} = \frac{D_o(\bar{\varphi}) + \delta B(m - 1/2, 3/2) (-\bar{\varphi})^m}{D_o(\bar{\varphi} = -1) + \delta B(m - 1/2, 3/2)}, \quad (2.4)$$

where the potential $\varphi(r)$, radius r and density $\rho(r)$ are made in dimensionless form using equations

$$\bar{\varphi}(r) = -\frac{\varphi(r)}{\sigma_c^2}, \quad (2.5a)$$

$$\bar{r} = r \sqrt{\frac{4\pi G \rho_c}{\sigma_c^2}}, \quad (2.5b)$$

$$\bar{\rho}(r) = \frac{\rho(r)}{\rho_c}. \quad (2.5c)$$

where the variables with subscript c corresponding to the time-dependent variables in self-similar analysis (Ito, 2020a) and the variables at a certain time t_c of (Ito, 2020b). The boundary conditions for Poisson equation (2.4) are

$$\bar{\varphi}(\bar{r} = 0) = 1, \quad \frac{d\bar{\varphi}}{d\bar{r}}(\bar{r} = 0) = 0. \quad (2.6)$$

Since $\bar{\varphi}$ is an independent variable for the ss-OAFP model, following the method of inverse mapping (Ito et al., 2018), we solved the Poisson equation in its inverse form for $\mathcal{R}(\bar{\varphi})$

$$\mathcal{R} \frac{d^2\mathcal{R}}{d\bar{\varphi}^2} - 2 \left(\frac{d\mathcal{R}}{d\bar{\varphi}} \right)^2 = \left(\frac{d\mathcal{R}}{d\bar{\varphi}} \right)^3 \frac{D_o(\bar{\varphi}) + \delta B(m - 1/2, 3/2) (-\bar{\varphi})^m}{D_o(\bar{\varphi} = -1) + \delta B(m - 1/2, 3/2)}. \quad (2.7)$$

The numerical integration of the Poisson equation provided the density profile (Figure 2) and m.f. potential (Figure 3) for an optimal index $m = 3.9$. (The reason why $m = 3.9$ is an optimal choice is explained in Section 2.4.) In the figures the value of δ spans 10^{-5} through 10^3 . For large $\delta > 1$, the profiles show almost the same morphology since they behave like a polytrope of $m = 3.9$. On one hand, the profiles approach the ss-OAFP model for small $\delta (\lesssim 10^{-2})$.

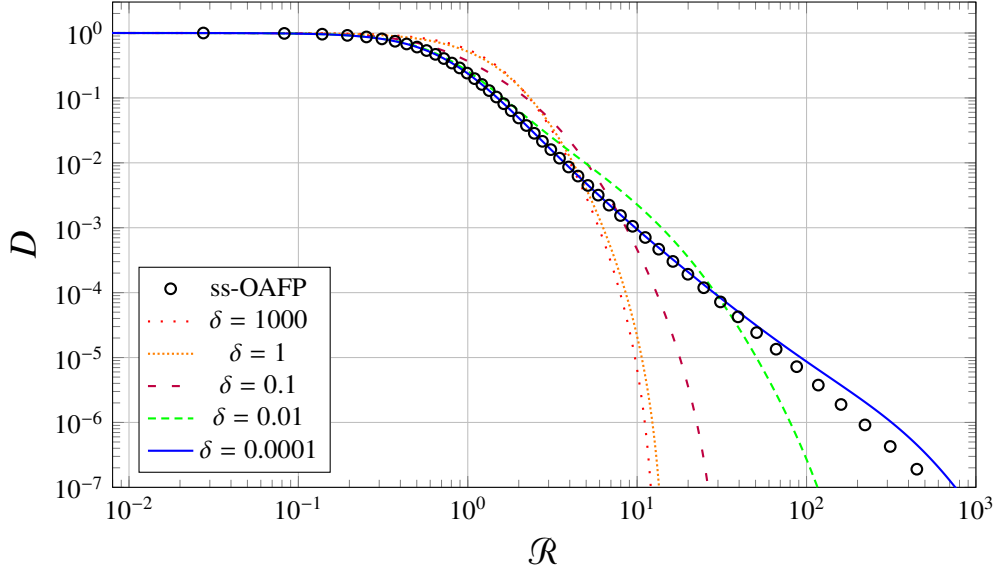


Figure 2: Dimensionless density $D(\mathcal{R})$ of the energy-truncated ss-OAFP model for different δ . The corresponding profile of the ss-OAFP model is also depicted.

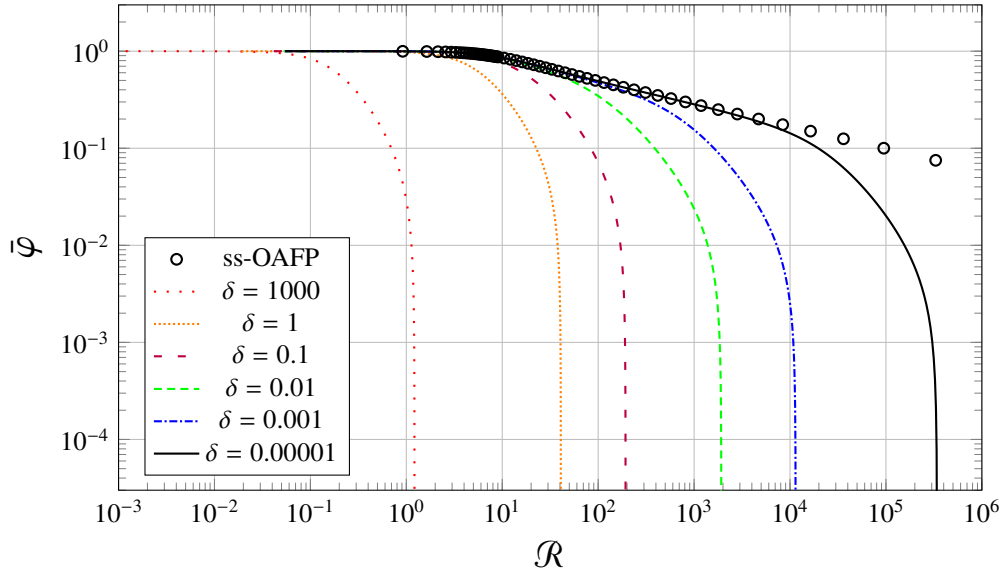


Figure 3: Dimensionless potential $\bar{\varphi}(\mathcal{R})$ of the energy-truncated ss-OAFP model. The corresponding potential of the ss-OAFP model is also depicted.

For application of density profile to globular clusters, one needs to convert the density profile $D(\bar{\varphi})$ to the projected density profile using the following expression

$$\Sigma(r) = 2 \int_0^\infty \frac{D(\varphi)}{\sqrt{1 - (r/r')^2}} dr', \quad (2.8)$$

and the corresponding inverse form with dimensionless variables is

$$\Sigma(\bar{\varphi}) = -2 \int_0^{\bar{\varphi}} \sqrt{\frac{1 - \mu_{\mathcal{R}}(\bar{\varphi}, \bar{\varphi}')}{1 + \mu_{\mathcal{R}}(\bar{\varphi}, \bar{\varphi}')}} \left[-2 \frac{dD}{d\bar{\varphi}'} \frac{\mathcal{R}(\bar{\varphi}')}{S(\bar{\varphi}')} + D(\bar{\varphi}') S(\bar{\varphi}') \frac{1 + 2\mu_{\mathcal{R}}(\bar{\varphi}, \bar{\varphi}')}{1 + \mu_{\mathcal{R}}(\bar{\varphi}, \bar{\varphi}')} \right] d\bar{\varphi}', \quad (2.9)$$

where $\mu_{\mathcal{R}}(\bar{\varphi}, \bar{\varphi}') \equiv \mathcal{R}(\bar{\varphi}')/\mathcal{R}(\bar{\varphi})$ and $S \equiv -d\mathcal{R}/d\bar{\varphi} (< 0)$. Figure 4 depicts the projected density profiles for different δ . As δ decreases the slope of $\mathcal{R}^{-1.23}$ in the inner halo develops more clearly (as expected from the asymptotic density profile for the ss-OAFP model; $D \propto \mathcal{R}^{-2.23}$). This power law occurs at radii between $\mathcal{R} \sim 10$ and $\mathcal{R} \sim 100$ for $\delta = 10^{-4}$ though, one also can find a similar power law for larger δ . For $\delta = 10^{-2}$ and 10^{-3} , Σ shows power-law-like structures $\mathcal{R}^{-1.0} \sim \mathcal{R}^{-1.1}$ at radii between $\mathcal{R} \sim 1$ and $\mathcal{R} \sim 10$. This property is a desirable feature to fit our model to the projected density profiles of PPC clusters whose projected density has similar power law profiles near the core (e.g. Djorgovski and King, 1986; Lugger et al., 1995).

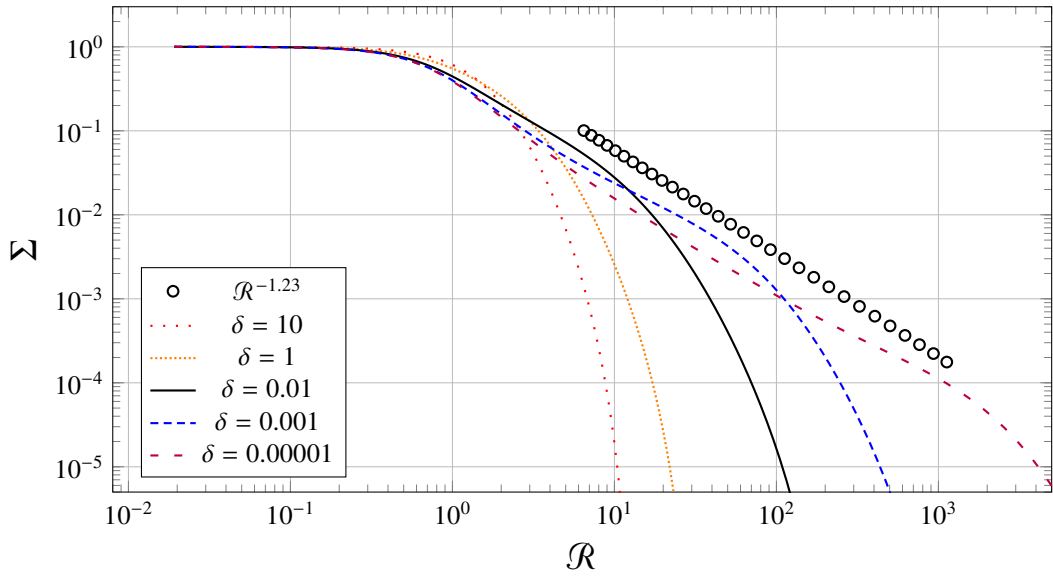


Figure 4: Projected density Σ of the energy-truncated ss-OAFP model for different δ . The power-law $R^{-1.23}$ corresponds to the asymptotic approximation of the ss-OAFP model as $R \rightarrow \infty$.

2.3. Regularization for the concentration and King radius

The energy-truncated ss-OAFP model is different from the King model in the sense of how concentration and core radius depend on the dimensionless central potential K , hence one must properly regularize the structural parameters for comparison. The King model (King, 1966) may be written in the following form by regularizing the m.f. potential as $\bar{\varphi} \equiv \bar{\varphi}/K$

$$\frac{d^2 \bar{\varphi}}{d\bar{r}^2} + \frac{2}{\bar{r}} \frac{d\bar{\varphi}}{d\bar{r}} - \frac{1}{K} \frac{I(\bar{\varphi})}{I(1)} = 0, \quad (2.10)$$

where the function $I(x)$ is

$$I(x) = \exp(x) \operatorname{erf}(\sqrt{x}) - \sqrt{\frac{4x}{\pi}} \left[1 + \frac{2x}{3} \right], \quad (2.11)$$

where $\operatorname{erf}(x)$ is the error function; $\operatorname{erf}(x) = 2 \exp[x^2] \int_0^x \exp[-x^2] dx / \sqrt{\pi}$. Due to the K -dependence of the equation, as $K \rightarrow 0$ the concentration is also $c \rightarrow 0$. Of course, the minimum radius of the King model can be the tidal radius of polytrope of $m = 2.5$, that is 5.355275459... (e.g. Boyd, 2011) if one regularizes the radius as $\bar{r} = \sqrt{K} \bar{r}$. On one

hand, the ss-OAFP model dose not depend on K . To find the same value of concentration (if necessary) or at least the same order as that of the King model, one must regularize the core radius and concentration⁵ as follows

$$\bar{r}_{\text{Kin}} \equiv \frac{r_{\text{Kin}}}{\sqrt{K^{(m)}}}, \quad (2.12a)$$

$$\bar{c} \equiv \log \left[\frac{r_{\text{tid}}}{r_{\text{King}}} \sqrt{K^{(m)}} \right], \quad (2.12b)$$

where $K^{(m)}$ is the dimensionless central potential that can be given when the the tidal radius divided by \sqrt{K} of the King model is approximately the same as that of polytrope of m . Using this regularization, one can obtain the concentration of the energy-truncated ss-OAFP model. For example, if $m = 3.9$ is chosen, then the tidal radius of the polytrope of $m = 3.9$ is 13.4731. In this case, K of the King model must be chosen so that the tidal radius divided by \sqrt{K} of the King model is close to 13.4731. This can be achieved when $K = 4.82$ with the tidal radius 13.444 (based on our calculation). Hence, $K^{(m)} = 4.82$ for $m = 3.9$. (We show in Section 2.4 that the concentrations calculated by this scaling are reasonably close to those of the King model.) Figure 5 depicts the concentration \bar{c} for $m = 3.9$. As δ increases, the concentration approaches a constant value that is corresponding to the concentration of polytrope of $m = 3.9$. The present focus is $\delta < c_4^*(= 0.3032)$ with which the energy-truncated ss-OAFP model approaches the ss-OAFP model and differentiates itself from the isothermal sphere and King model. The corresponding concentration is $\bar{c} > 1.45$. On one hand, our model is expected to behave like the King model for $1 < \bar{c} < 1.45$ and like a polytrope of $m = 3.9$ in the limit of $\bar{c} \rightarrow 1$.

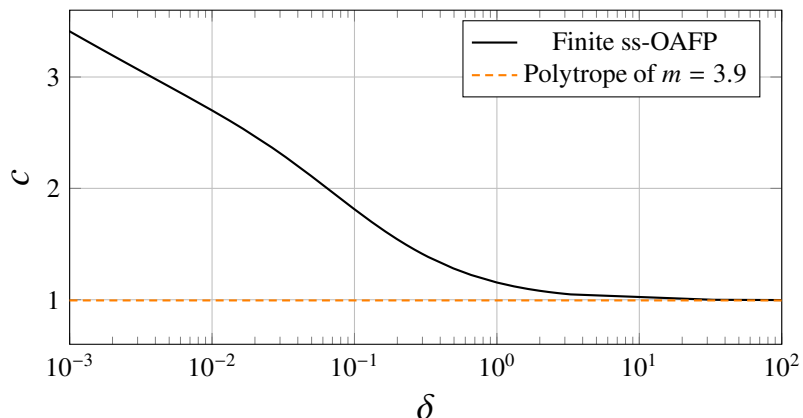


Figure 5: Concentration of the energy-truncated ss-OAFP model. The horizontally dashed line represents the concentration for polytropic sphere of $m = 3.9$.

2.4. An optimal choice for polytropic index: $m = 3.9$

We determined the index m to be 3.9 in the energy-truncated ss-OAFP model after having preliminarily applied the model to the projected surface densities of six KM clusters and a PCC cluster that we chose. For application of our model to KM clusters, we chose an optimal value for the index m so that our model gives the same order of the tidal radius, King radius and exponential of concentration of six chosen KM clusters as those reported in the previous works. Initially, we expected $m = 2.5$ could be an optimal choice for the energy-truncated ss-OAFP model following (Spitzer and Shapiro, 1972) though, it was not the case. The useful values were found in $3.5 < m < 4.4$ with which our model reasonably fits the projected surface densities for KM clusters reported in (Kron et al., 1984; Noyola and Gebhardt, 2006; Miocchi et al., 2013) (See Appendix A). Among the values of m , we chose 3.9 as an optimal value for the present work. This is since it provides the same order of magnitudes of structural parameters for six chosen clusters as that of the existing works based on the King model, as shown in Table

⁵The tidal radius for the energy-truncated ss-OAFP model should not be regularized since it is still the radius at which the projected density reaches zero which can be found after the model is properly fitted to the projected structural profile of a globular cluster on graph.

1. The table provides the results for fitting of our model with $m = 3.9$ to six Milky Way globular clusters reported in (Kron et al., 1984). Only the six clusters are reported in all the compilation works (Peterson and King, 1975; Kron et al., 1984; Chernoff and Djorgovski, 1989; Trager et al., 1993; Miocchi et al., 2013) that we chose to compare this time. Miocchi et al. (2013) did not show the numeric values of projected density profiles but the six clusters in Table 1 have approximately the same maximum radius points of the projected density profiles on graphs reported in (Kron et al., 1984). While many of the compilation works based on the King model are inhomogeneous surveys in the sense they depend on different instruments, photometry methods and statistical analyses, the structural parameters obtained from our model are reasonably close to the results of the compilation works. On one hand, If $m < 3.8$ or $m > 4.3$ is chosen for the fitting, the magnitudes of the structural parameters are less or greater by over a factor of ten from the compilation works' results. Interestingly, our structural parameters are close to those obtained from the King model rather than the Wilson model (Wilson, 1975); the latter has a higher index m than the former in the limit of $K \rightarrow 0$. The Wilson model (Wilson, 1975) relies on the polytrope of $m = 3.5$ in the limit $K \rightarrow 0$ which provides greater values of the structural parameters since the polytrope of $m = 3.5$ reaches further in radius compared to the polytrope of $m = 2.5$ that the King model follows in the same limit (e.g. Chandrasekhar, 1939). The reason why our model does not overestimate the structural parameters with high $m (= 3.9)$ would be that the density profile of the ss-OAFP model more rapidly decays compared to the isothermal sphere in the inner halo (Figure 1). One can find in Appendix A the energy-truncated ss-OAFP model with $m = 3.9$ reasonably fitted to the projected structural profiles of KM clusters reported in (Kron et al., 1984; Noyola and Gebhardt, 2006; Miocchi et al., 2013).

Another reason why we chose $m = 3.9$ is that the energy-truncated ss-OAFP model with $m = 3.9$ agreeably fits the relatively new data for NGC 6752 reported in (Ferraro et al., 2003). Ferraro et al. (2003) provided data points and error bars of the projected surface density for NGC 6752, which is convenient to test our model (since we do not have to artificially extract data from their graph.). In their work, the King model does not well fit the central part of the projected density profile since the cluster is one of (possible) PCC clusters with a power-law profile like core. Hence, following (Lugger et al., 1995), they employed modified power law profile like $\sim (1 + (r/3.1)^2)^{-0.525}$ where r is measured in log [arcsec]. This well fits the central part as shown in Figure 6 (left top). On one hand, our model with $m = 3.0$ is not close to the morphology of the cluster at all on the figure. We, however, can more reasonably fit our model to the same data with greater m ; especially, for $m = 4.2$ the model well fits the data except in the tail of the cluster. Even with $m = 3.9$, one can find a reasonable fit to the data, hence the present work chose $m = 3.9$ to consistently accumulate the data for both KM clusters and PPC clusters.

	NGC 1904			NGC 2419			NGC 6205		
	c	r_c	r_{tid}	c	r_c	r_{tid}	c	r_c	r_{tid}
Finite ss-OAFP									
The present work based on data of (Kron et al., 1984)	1.86	0.191	13.9	1.24	0.410	7.16	1.54	0.779	27.0
King model									
(Miocchi et al., 2013)	1.76	0.15	9.32	1.51	0.27	9	1.32	0.825	18.5
(Harris, 1996, (2010 edition))	1.70	0.16	8.0	1.37	0.32	7.5	1.53	0.62	21.0
(Trager et al., 1993)	1.72	0.159	8.35	1.4	0.348	8.74	1.49	0.875	27.0
(Chernoff and Djorgovski, 1989)	1.90	0.132	10.5	1.6	0.373	14.8	1.35	0.745	16.7
(Kron et al., 1984)	1.75	0.178	10.0	1.00	0.398	3.98	1.25	0.83	14.8
(Peterson and King, 1975)	1.60	0.27	10.7	1.41	0.42	10.7	1.55	0.76	26.9
Wilson model									
(Miocchi et al., 2013)	2.14	0.18	28	1.73	0.32	20	1.77	0.841	57

	NGC 6229			NGC 6341			NGC 6864		
	c	r_c	r_{tid}	c	r_c	r_{tid}	c	r_c	r_{tid}
Finite ss-OAFP									
The present work based on data of (Kron et al., 1984)	1.45	0.178	5.00	1.68	0.314	15.0	1.83	0.116	7.85
King model									
(Miocchi et al., 2013)	1.65	0.13	6.12	1.74	0.243	13.9	1.79	0.082	5
(Harris, 1996, (2010 edition))	1.50	0.12	3.79	1.68	0.26	12.4	1.80	0.09	6.19
(Trager et al., 1993)	1.61	0.13	5.39	1.81	0.235	15.2	1.88	0.096	5.68
(Chernoff and Djorgovski, 1989)	1.40	0.167	4.19	1.70	0.132	6.64	1.85	0.084	5.91
(Kron et al., 1984)	1.25	0.173	3.08	1.50	0.308	9.75	1.75	0.095	5.34
(Peterson and King, 1975)	1.41	0.22	5.62	1.78	0.275	16.6	N/A	0.12	> 3.2
Wolley model									
(Miocchi et al., 2013)	1.82	0.16	12.0	2.17	0.33	46	2.38	0.095	25

Table 1: Concentration and core- and tidal- radii obtained from the energy-truncated ss-OAFP model. The structural parameters are compared to the previous compilation works based on the King- and Wilson- models.

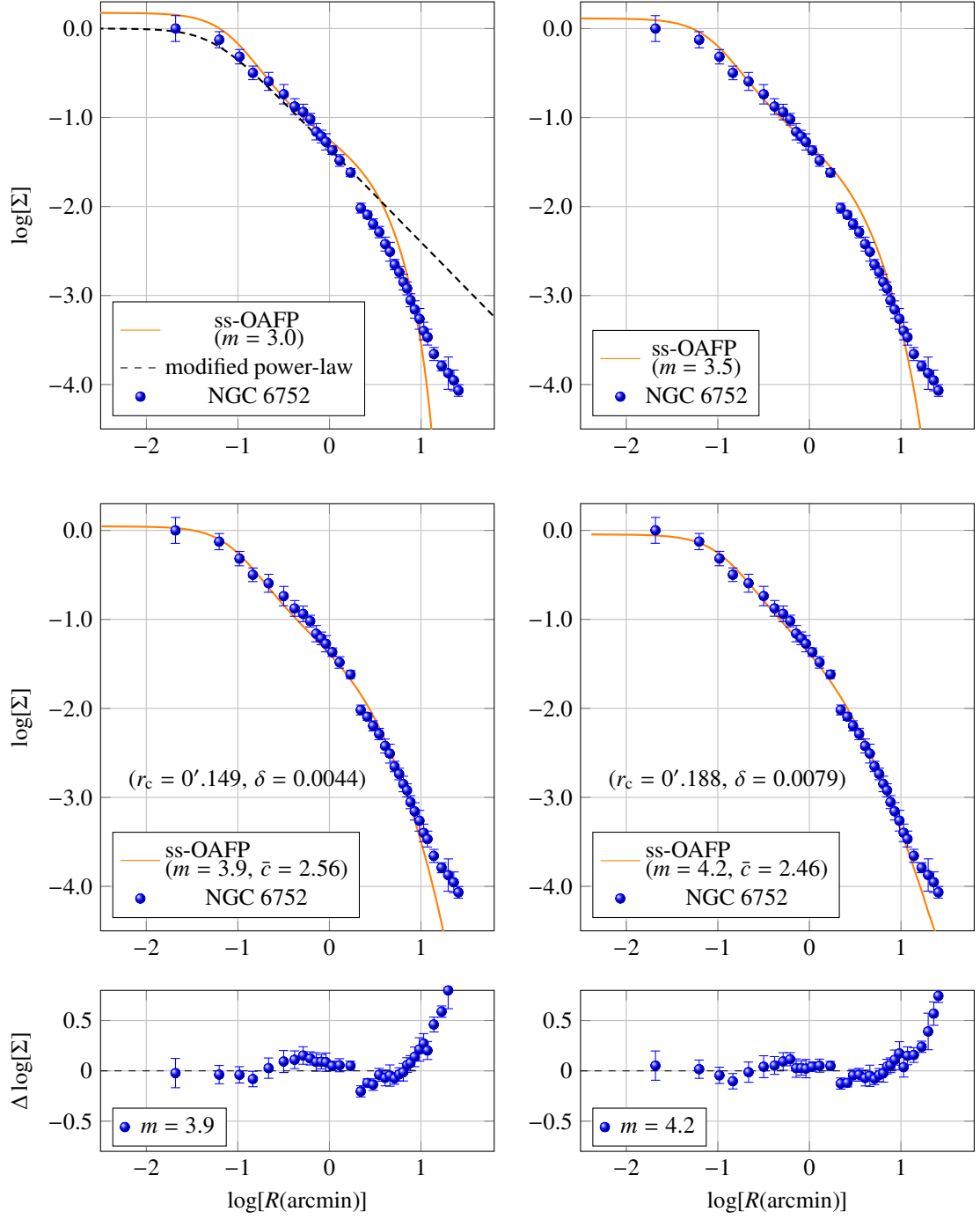


Figure 6: Fitting of energy-truncated ss-OAFP model to the projected density profile of NGC 6752 (Ferraro et al., 2003) for different m . The unit of Σ is number per square of arcminutes and Σ is normalized so that the density is unity at the smallest radius of data points. In the legends, (c) means PCC cluster as judged so in (Ferraro et al., 2003). In the left top panel, double-power law profile is depicted as done in (Ferraro et al., 2003). In the two bottom panels, $\Delta \log[\Sigma]$ for $m = 3.9$ and $m = 4.2$ depicts the corresponding deviation of Σ from our model.

3. Fitting of the ss-OAFP model to PCC clusters

The energy-truncated ss-OAFP model with $m = 3.9$ reasonably fits to the projected structural profiles of PCC clusters with resolved cores at $R \lesssim 1$ arcminute. Other than NGC 6752, we also have access to numerical data of the projected density profile for NGC 6397 from (Drukier, 1995). Our model reasonably fits to the density for NGC 6397 with $\chi_v^2 = 1.52$ (Figure 7) where the reduced chi-square is defined as follows

$$\chi_v^2 = \sum \frac{\chi^2}{n_{d.f.}}, \quad (3.1)$$

where χ^2 is the chi-square value between the observed data and our model, and $n_{d.f.}$ is the degree of freedom. We chose $n_{d.f.} = 3$ in the same way as the King model since index m of our model is fixed to 3.90. Since we did not have access to numerical values for the rest of the projected density profiles for PCC clusters reported in (Djorgovski and King, 1986; Lugger et al., 1995), our error analysis becomes less trustful hereafter. Yet it appears enough to capture the applicability of our model to the PCC clusters. For example, Meylan and Heggie (1997) introduced NGC 6388 and Terzan 2 as an example for a KM cluster and PCC cluster by citing the surface brightness profiles of the clusters from Djorgovski and King (1986)'s work though, the energy-truncated ss-OAFP model reasonably fits both density profiles at radii $R \lesssim 1$ arcminute (Figure 8). (As discussed in Section 5, to fit our model to densities at $10 \sim 100$ arcminutes the value of m is to be $m \gtrsim 4.2$.) In a similar way to NGC 6752 and NGC 6397, we applied our model to PCC clusters with resolved cores and some clusters with unresolved cores reported in (Djorgovski and King, 1986; Lugger et al., 1995) (See Appendix C in which the 'possible' PCC clusters reported in (Kron et al., 1984) are also fitted). Table 2 shows the values of χ_v^2 for both KM- and PCC- clusters that we obtained the uncertainties in observed densities from the numerical values or graphs. The result is obvious that the profiles of the KM clusters are well fitted by the ss-OAFP model for all the data points given. On one hand, for PCC clusters, the model fits to only clusters with resolved cores reported in (Lugger et al., 1995). For example, the PCC clusters with partially-resolved cores (NGC 6453, NGC 6522 and NGC 7099) and resolved cores (NGC 6397 and NGC 6752) are reasonably fitted at $R \lesssim 1$ arcminumte with $\chi_v^2 \lesssim 2$. Even a PCC cluster with unresolved core (NGC 6342) can be reasonably fitted in a similar way, while the present work does not account for the 'seeing-effect' that comes from the finiteness of the seeing-disk. The structural profiles of the rest of PCC clusters with unresolved cores (e.g. NGC 5946 and NGC 6624) were hopeless to be fitted even only for the cores, whose central parts have steeper power-law profiles compared to our model. This was expected since the present model does not correctly include the effect of binaries whose heating effect is possibly inefficient to provide resolved cores.

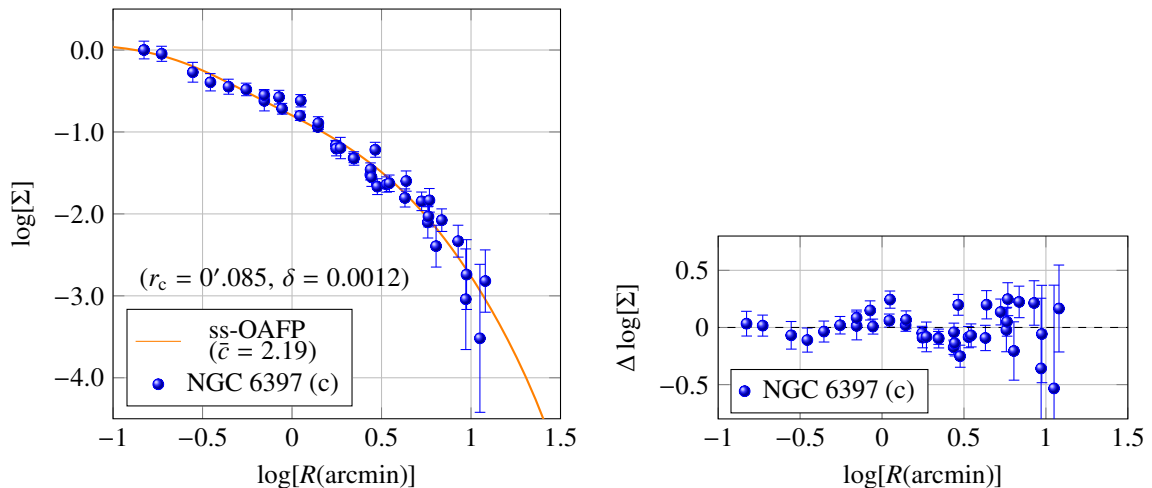


Figure 7: Fitting of energy-truncated ss-OAFP model ($m = 3.9$) to the projected surface density of NGC 6397 reported in (Drukier et al., 1993). The unit of Σ is number per square of arcminutes and Σ is normalized so that the density is unity at smallest radius for data. In the legends, (c) means PCC cluster as judged so in (Djorgovski and King, 1986). $\Delta \log[\Sigma]$ is the corresponding deviation of Σ from the model on log scale.

KM cluster	χ_v^2	N_b	PCC cluster	χ_v^2	N_b
NGC 288	0.45	0	NGC 6342	1.73	3
NGC 1851	0.56	0	NGC 6397	1.52	0
NGC 5466	2.07	0	NGC 6453	1.89	5
NGC 6121	0.72	0	NGC 6522	2.52	5
NGC 6205	1.05	0	NGC 6558	2.17	5
NGC 6254	0.57	0	NGC 6752	2.00	6
NGC 6626	0.47	0	NGC 7099	2.12	2
NGC 6809	0.44	0	Trz 1	2.41	5
Pal 3	0.06	0	Trz 2	1.94	0
Pal 4	0.34	0			
Pal 14	0.31	0			
Trz 5	2.23	0			

PCC cluster	χ_v^2	N_b
NGC 5946	6.75	5
NGC 6624	7.18	5

Table 2: Values of χ_v^2 and number of points discarded from the calculation. The data used for fitting to KM clusters are from (Miocchi et al., 2013), to NGC 6397 from (Drukier et al., 1993), to Terzan 2 from (Djorgovski and King, 1986), to NGC 6752 from (Ferraro et al., 2003) and to the rest of PCC clusters from (Lugger et al., 1995). N_b is the number of data points at large radii excluded from calculation.

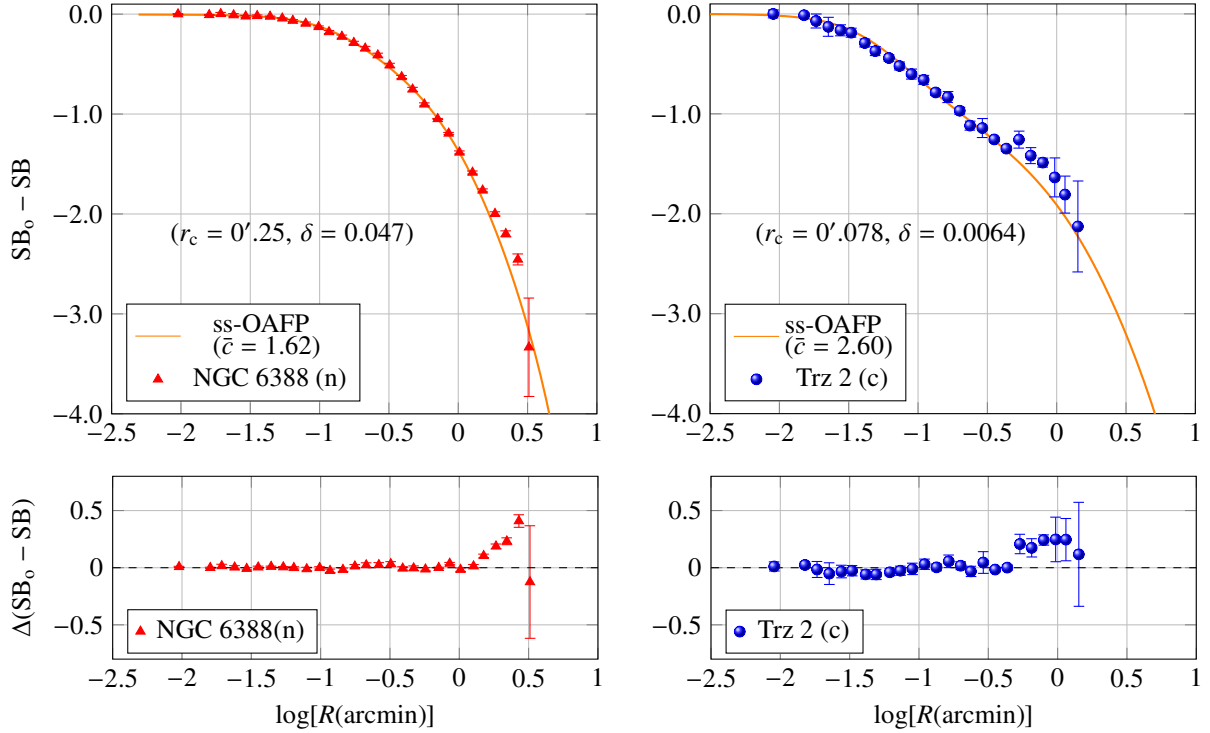


Figure 8: Fitting of the energy-truncated ss-OAFP model ($m = 3.9$) to the surface brightness profiles of Terzan 2 and NGC 6388 reported in (Djorgovski and King, 1986). The unit of the surface brightness (SB) is B magnitude per square of arcseconds. The brightness is normalized by the magnitude SB_0 at the smallest radius point. In the legends, (n) means normal or KM cluster and (c) means PCC cluster as judged so in (Djorgovski and King, 1986). $\Delta(SB_0 - SB)$ is the corresponding deviation of $SB_0 - SB$ from the model.

4. (Main result) Relaxation time and completion rate of core collapse against concentration including PCC clusters with resolved cores

Concentration \bar{c} is a possible measure to characterize the states of globular clusters in the relaxation evolution especially for the cores, hence the present section compares \bar{c} to the core relaxation time and completion rate of core collapse. Since the energy-truncated ss-OAFP model can reasonably apply not only to KM clusters (Appendix A) but also to PCC clusters (Appendix C), one may systematically discuss their relationship. We first discuss here how the core relaxation time depends on the concentration. Figure 9(a) depicts the characteristics of the core relaxation time $t_{c.r.}$ against the concentration \bar{c} and Figure 9(b) the corresponding characteristics based on King model reported in (Harris, 1996, (2010 edition)). All the relaxation times on both figures for PCC- and KM- clusters are the values reported in (Harris, 1996, (2010 edition))’s catalog. In the catalog, some of concentrations are depicted as ‘2.50c’ for clusters whose projected structural profiles are not well fitted by the King model. Hence, we simply assumed in Figure 9 (b) the concentration of such clusters is 2.50. In Figure 9(b) the relaxation time decreases with increasing concentration c for KM clusters, yet it is not clear if PCC clusters have the same tendency. On one hand, Figure 9(a) shows not only the relaxation time decreases with concentration \bar{c} for KM clusters but also the time drops down almost vertically for PCC clusters for long relaxation time. This tendency well captures the nature of PCC clusters whose projected profiles can be close to the ss-OAFP model in complete-collapsed state but still similar to the King model (KM clusters) in expansion phase after their cores collapse.

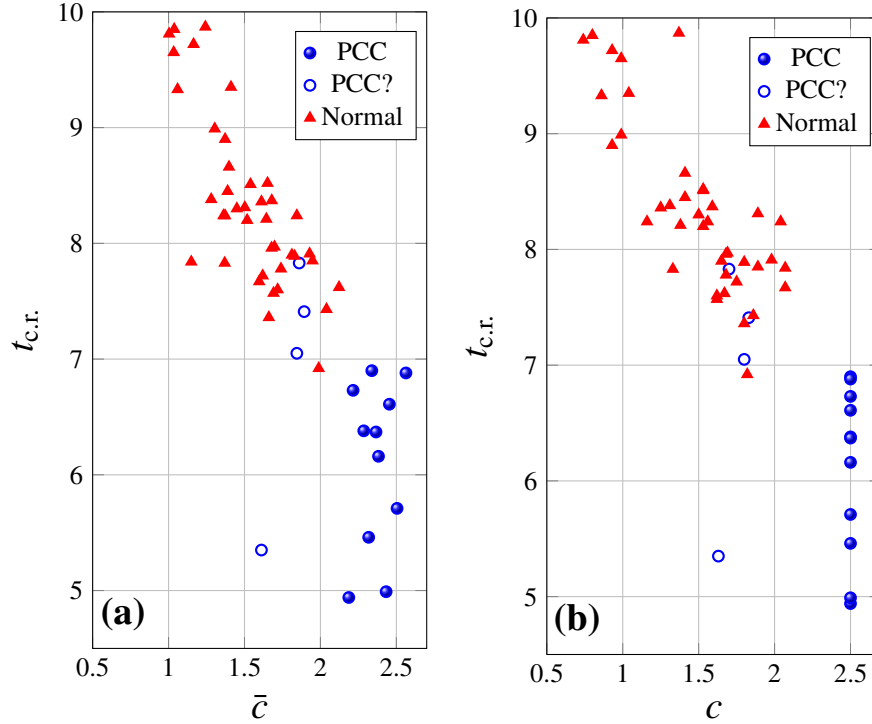


Figure 9: Core relaxation time against (a) concentration \bar{c} obtained from the energy-truncated ss-OAFP model ($m = 3.9$) applied to PCC- and KM-clusters and (b) concentration c based on the King model reported in (Harris, 1996, (2010 edition)).

To see the completion rate of core collapse, we use the formula employed in (Lightman, 1982)

$$\eta_c \equiv \frac{t_{o,age}}{t_{c.r.o}} \equiv \frac{t_{o,age}}{t_{c.r.}} \frac{-(1 + Aq_0) + \sqrt{(1 + Aq_0)^2 + 4ABq_0}}{2Bq_0} \quad (4.1)$$

where $A = 35$, $B = 4.8$ and $q_0 = t_{o,age}/t_{c.r.}$ with $t_{o,age}$ being the order of age of clusters $\sim 10^{10}$ years. The time $t_{c.r.o}$ is the estimated relaxation time at the beginning of evolution of each cluster based on N -body simulation. Figure

10 (a) shows the completion rate against concentration \bar{c} obtained from the energy-truncated ss-OAFP model. The majority of data plots are within the region between lines $\eta_c = 0.75(\bar{c} - 2.0) + 1.05$ and $\eta_c = 0.75(\bar{c} - 2.0) + 0.40$ that are empirical lines of equation, not based on physical arguments. Figure 10 (b) shows that the corresponding characteristics of η_c against concentration c based on the King model, and the same two lines reasonably include the majority of data points between them. From Figure 10 (a), one can find several conclusion. (i) The criterion explained in (Meylan and Heggie, 1997) still works that clusters with $c > 2.0$ are PCC clusters but if the completion rate is above 0.8 (ii) Clusters with over a completion rate of 0.8 are PPC clusters except for a cluster NGC 6517. (iii) KM clusters with high concentration ($c \geq 2.0$) in (Harris, 1996, (2010 edition))’s catalog are reasonably close to the other KM stars in the figure and their concentration are lowered to values smaller than 2.0, while our model suggests two KM clusters (NGC 1851 and NGC 6626) with high concentration ($\bar{c} \geq 2.0$) have morphology close to complete core-collapse state. (iv) A PCC cluster (NGC 6544) differentiates itself from the KM- and PCC- clusters in the sense that NGC 6544 has a high completion rate (0.989) compared to the KM clusters and a *very* low concentration ($\bar{c} = 1.61$) compared to the rest of PCC clusters. Hence, the cluster may be a good candidate for search of a PPC cluster that may have one of most expanded cores, while the cluster was judged only as ‘possible PCC’ in (Djorgovski and King, 1986). (v) Our model with $\bar{c} \approx 1$ fits the projected structural profiles of low-concentration clusters, which infers the clusters may have structures similar to polytrope of $m \approx 3.9$. The conclusion (i) simply confirmed an expected property of core collapse process and conclusions (ii) through (iv) require a detail case study for each cluster, which is out of scope in the present work. Hence, we further discuss only the conclusion (v) in detail in Section 5.

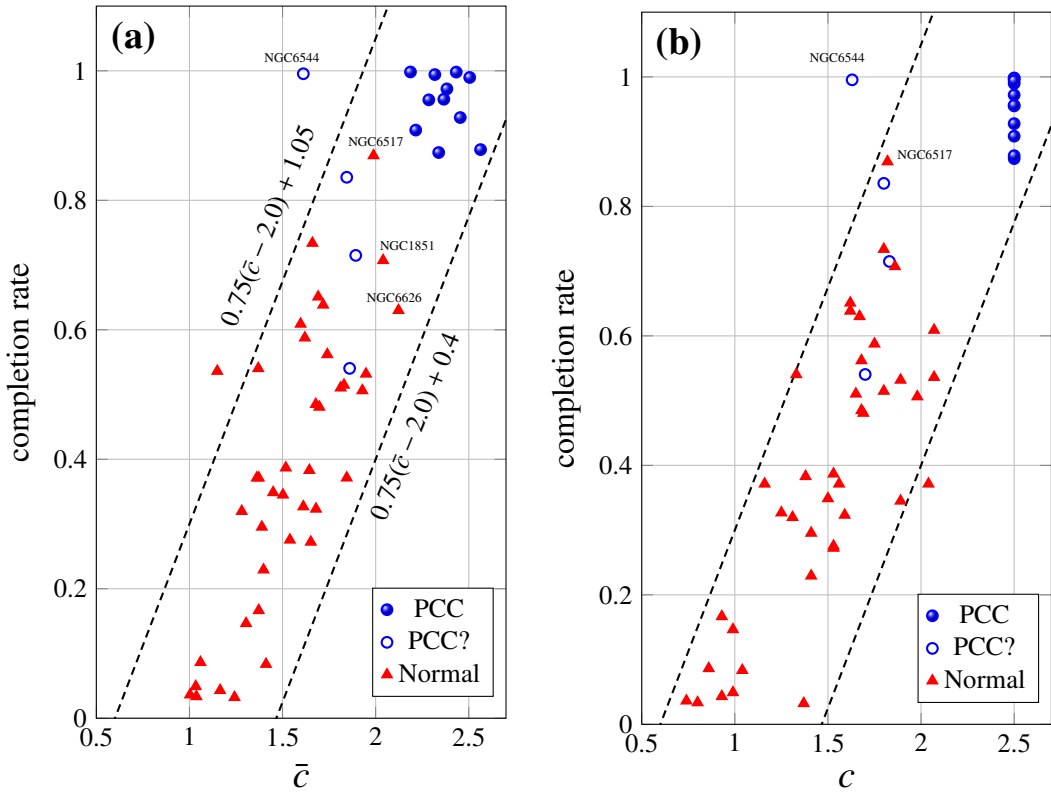


Figure 10: Completion rate of core collapse against (a) concentration \bar{c} based on the energy-truncated ss-OAFP model with $m = 3.9$ and (b) concentration c based on the King model reported in (Harris, 1996, (2010 edition)).

5. Discussion

The present section discusses the three topics that we could not detail in the main results; (i) a possible use of the energy-truncated ss-OAFP model with high index m (higher than $m = 3.9$) to the structural profiles of globular clusters

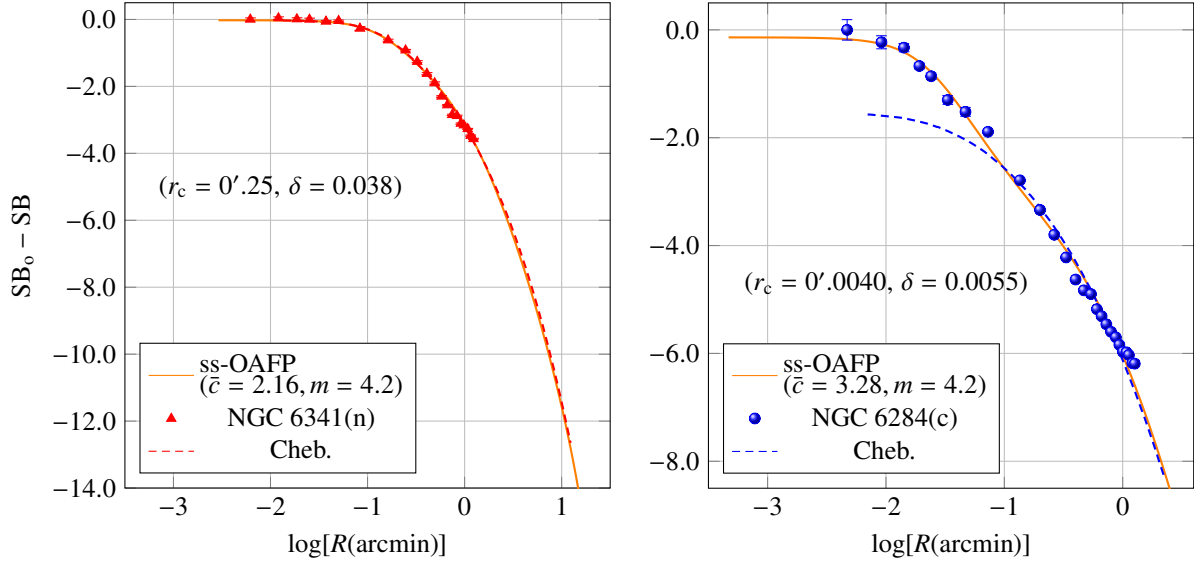


Figure 11: Fitting of the energy-truncated ss-OAFP model to the surface brightness profiles of NGC 6284 and NGC 6341 reported in (Noyola and Gebhardt, 2006). ‘Cheb.’ means the Chebyshev approximation of the surface brightness reported in (Trager et al., 1995). The unit of the surface brightness (SB) is V magnitude per square of arcseconds. The brightness is normalized by the magnitude SB_0 at the smallest radius point. In the legends, (n) means normal or KM cluster and (c) means PCC cluster as judged so in (Djorgovski and King, 1986).

in a broad range of radii $10^{-2} \sim 10^1$ arcminutes (Section 5.1), (ii) an application limit and an approximated form of our model (Section 5.2) and (iii) why our model can fit the projected structural profiles even for low-concentration ($\bar{c} \approx 1$) globular clusters (Section 5.3).

5.1. Fitting of the energy-truncated OAFP model to ‘whole’ projected density with higher index m

In the present section, we show that the energy-truncated ss-OAFP model with $m = 4.2$ well fits to the surface brightness profiles of some PCC clusters and KM clusters in a broad range of radii (approximately between 0.01 and 10 arcminutes). In the main result (Section 3), we employed $m = 3.9$ to consistently apply the model to various clusters though, as explained in Section 2.4, index m higher than 3.9 (e.g. $m = 4.2$) may provide a better fitting. Also, more recent surveys such as *Gaia 2* provided structural profiles with elongated outer halos for some clusters that can not be well fitted by the King model, rather the Wilson model showed a better fitting (de Boer et al., 2019). A similar situation was reported also in (Miocchi et al., 2013). Under the circumstances, we applied our model to the V-band magnitudes of globular clusters reported in (Noyola and Gebhardt, 2006) combined with those of (Trager et al., 1995)⁶. Following (Noyola and Gebhardt, 2006), we simply overlapped their magnitudes to those of (Trager et al., 1995). For example, Figure 11 shows the fitting of our model with $m = 4.2$ to the surface brightness profile of NGC 6341 and NGC 6284; the former is a KM cluster and the latter PCC. Following the fitting done in (Noyola and Gebhardt, 2006), we fitted our model to the surface brightness so that in the outer halo our model fits the data plots (Chebyshev approximation) of (Trager et al., 1995) rather than the corresponding plots of (Noyola and Gebhardt, 2006). We need more realistic effects (e.g. mass function) to more reasonably fit our model to NGC 6284 though, our model appears capable to capture the structure (core and tidal radius) of the cluster. For the rest of fitting, see Appendix A.3 for KM clusters and Appendix B.3 for PCC clusters in which we did not include some clusters whose central cores have a negative slope reported in (Noyola and Gebhardt, 2006). For PCC clusters, we needed our model only with $m = 4.2$ while for KM clusters we needed indexes higher than $m = 4.2$.

⁶Unfortunately, we did not have an access to data of (de Boer et al., 2019) and were not able to employ *WebPlotDigitizer* to extract their data since many of their data plots and error bars are overlapped each other.

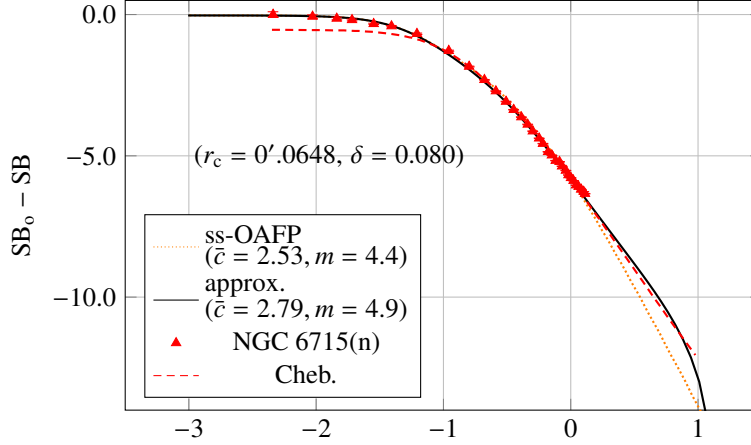


Figure 12: Fitting of the energy-truncated ss-OAFP model and its approximate form to the surface brightness of NGC 6715 reported in (Noyola and Gebhardt, 2006). ‘Cheb.’ means the Chebyshev approximation of the surface brightness reported in (Trager et al., 1995). The core radius r_c and δ in the figure were acquired from the approximated form. The unit of the surface brightness (SB) is V magnitude per square of arcseconds. The brightness is normalized by the magnitude SB_0 at the smallest radius point. In the legends, (n) means normal or KM cluster as judged so in (Djorgovski and King, 1986).

5.2. Application limit and an approximated form of the energy-truncated ss-OAFP model

The energy-truncated ss-OAFP model suffers from unrealistically large tidal radii ($\sim 10^5$ arcminutes) beyond $m = 4.4$ and can not approach $m = 5$, which prevents one from fitting the model to some globular clusters, hence the present section introduces an approximated form of the model as a remedy. Sections 2.4, 3 and 5.1 showed the applicability of the energy-truncated ss-OAFP model to many globular clusters for $m = 3.9$ and $m = 4.2 \sim 4.4$ though, it turns out that some globular clusters have more elongated structures in the outer halos that our model can not reach. For example, Figure 12 shows the projected density of NGC 6715 (reported in (Noyola and Gebhardt, 2006)) fitted by the model with $m = 4.4$. The observed density has a calmer slope in the halo compared to our model. Our model can reach further large radii by increasing m , yet it turns out the tidal radius unrealistically diverges soon, for example, the tidal radius is approximately 10^5 arcminutes for $m = 4.4$ and $\delta = 0.01$. (Even the tidal radius of polytrope of $m = 4.5$ is approximately only 31.54.)

To resolve the unrealistically large tidal radius of the ss-OAFP model with high indexes m , we introduce an approximated form of the energy-truncated ss-OAFP model that well fits the structural profiles of Galactic globular clusters. First, one may see that the values of δ that fit to globular clusters are relatively high ($\delta > 0.004$) and they would not show a distinctive sign of the power-law profile of $\Sigma \propto r^{-1.23}$ in the inner halo (Recall Figure 3; the power law $r^{-2.23}$ in density profile is recognizable when the value of δ is small $\sim 10^{-3}$). This infers we may approximate the model by excluding the contribution from the asymptotic power-law profile ($\Sigma \propto r^{-1.23}$) in the halo. In fact, the density profile for the energy-truncated ss-OAFP model can be well fitted by the exponential profile $\exp[-13.88(1 + E)]$ for low energies $E < -0.7$ as shown in Figure 13 (a). In the figure the exact model switches from the exponential decay (isothermal sphere) to the power law decay (polytropic sphere) around $E = -0.72$ at which their values are still the same order. Accordingly we may define an approximate form of DF for our model as follows

$$\tilde{F}(E) = \frac{\exp[-13.88(1 + E)] + \delta(-E)^m}{\exp[-13.88] + \delta}. \quad (5.1)$$

where 13.88 is the value of the scaled escape energy χ_{esc} for complete core collapse. One needs to know the advantage and disadvantage of using the approximated model. This approximation would be handy in the sense that one does not have to resort to the inverse form of the Poisson equation unlike our exact model. Also, one can employ the scaled escape energy other than the 13.88 if considering χ_{esc} as a new parameter allowing four degrees of freedom⁷. One

⁷We have tried to employ the four parameters model though, the useful values of χ_{esc} with which the approximated model well fits globular

one hand, the approximated model should not be applied to PCC clusters at first place since the approximation can be reasonable when $\delta \gg 10^{-3}$ as shown in Figure 13 (b). In the figure, the projected density profiles of the exact and approximated models are almost identical for large $\delta = 0.1$ while they obviously deviate from each other for small δ . More importantly, the approximated model loses the physical significance to examine how close the states of globular clusters are to complete core collapse state. Yet, the approximated form well fits even for the elongated structure in the outer halo of NGC 6715 (Figure 12). The reason why the approximated model may take higher $m(> 4.4)$ is that the density profile follows the exponential decay $\exp[-\chi_{\text{esc}}(1 + E)]$ at large E , which shortens the tidal radius in a similar way that Woolley's model (Woolley, 1961) does. This can be seen in Figure 14 in which density profile D_a of the approximated model behaves like exponential function at large E . See Appendices A.3 and B.3 to find the rest of application of the approximated model to KM- and PCC- clusters in a broad range of radii.

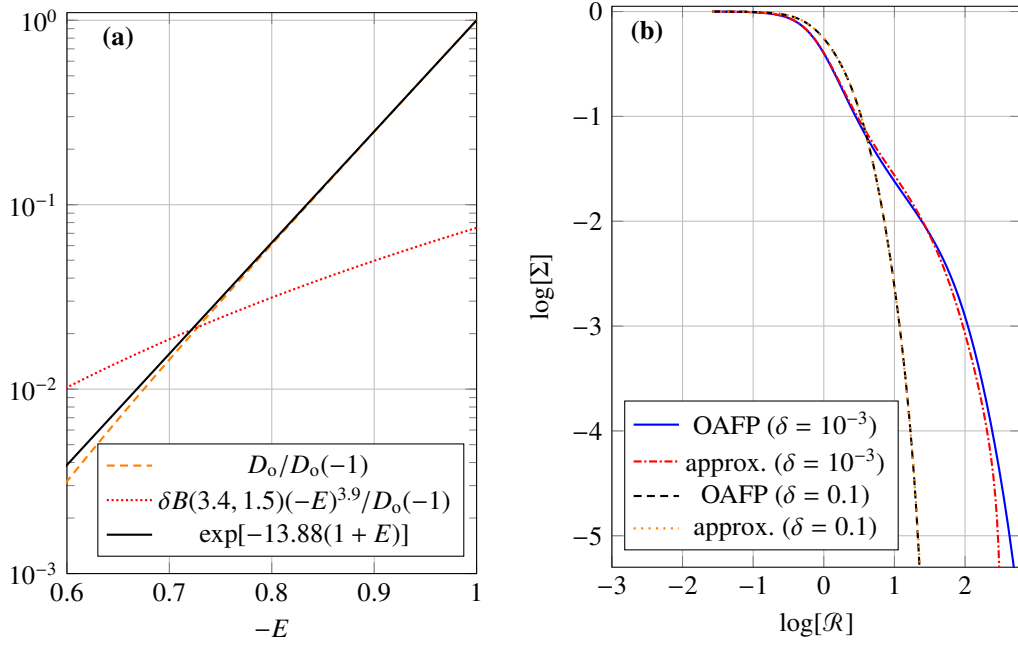


Figure 13: (a) Dimensionless density profiles D_o , $\exp[-13.88(1 + E)]$ and $\delta B(3.4, 1.5)(-E)^{3.9}/D_o(-1)$ for $\delta = 0.01$. (b) Projected density profiles for the energy-truncated ss-OAFP model and its approximation for $\delta = 0.1$ and $\delta = 0.001$. For the both, m is fixed to 3.9.

clusters were $\chi_{\text{esc}} \gtrsim 9$ holding the index m to 3.9. Less than those values, the morphology of the approximated model perfectly changed from the exact model and especially the approximated model with low $\chi_{\text{esc}} (\lesssim 9)$ could not fit PCC cluster at all; perhaps, this reflects the result of (Cohn, 1980) in which the signature of self-similarity and core collapse appears for $\chi_{\text{esc}} (\gtrsim 9)$.

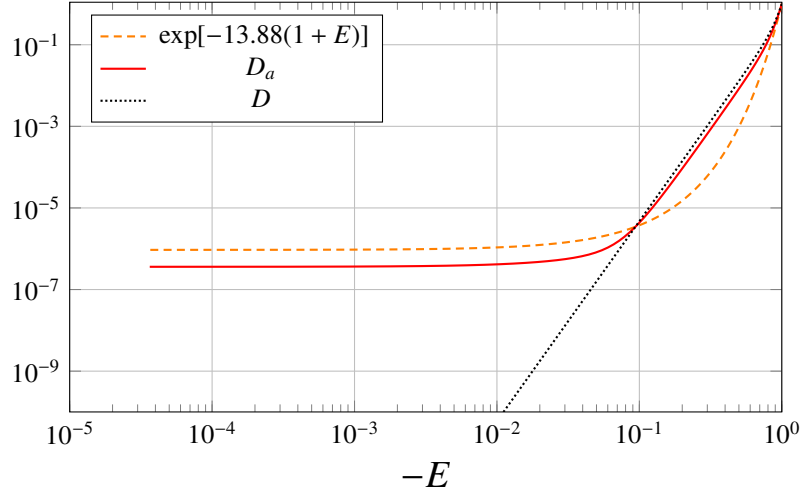


Figure 14: Density profiles D_0 of the energy-truncated ss-OAFP model, D_a of the approximated model and $\exp[-13.88(1 + E)]$.

5.3. Are low-concentration globular clusters like spherical polytropes?

The result of Section 4 indicates that low-concentration cluster may have projected structural profiles of polytropic spheres. This originates from the fact that some clusters (such as Palomar 3 and Palomar 4) have concentrations \bar{c} close to one, which means the projected structural profiles are like those of polytrope of $m = 3.9$ rather than isothermal sphere. Yet, fitting of the energy-truncated ss-OAFP model to those clusters are overfitting due to low number of data points and large size of error bars. Hence, to see whether the projected structural profiles of low-concentration globular clusters are polytropic, Appendix B shows the structural profile data (Kron et al., 1984; Trager et al., 1995; Miocchi et al., 2013) fitted by the polytropic sphere model. We found 18 polytropic globular clusters whose projected density and surface brightness profiles are well fitted by polytropic-sphere model. Here, we show the example for NGC 288 and NGC 6254; their concentrations based on the energy-truncated ss-OAFP model are 1.30 and 1.64 and those based on the King model is 1.0^8 and 1.41. NGC 288 is a good example for a polytropic globular cluster while NGC 6254 for a non-polytropic cluster. Figure 16 also depicts another example of polytropic-like globular cluster NGC 5139 whose surface brightness profile was reported in (Meylan, 1987). The central part of the cluster deviate from polytrope model due to the weak cusp though the inner- and outer- halos are well fitted by the polytropic sphere. In the rest, we consider possible physics arguments that the low-concentration globular clusters may have structures like polytropic spheres (Section 5.3.1) and its criticism (Section 5.3.2).

⁸Here, we consider the concentration of NGC 288 is 1.0 based on our fitting of the King model. We confirmed the concentrations c and values of χ_ν reported in Table 2 of (Miocchi et al., 2013) based on our calculation for the clusters that we cited here, but not for NGC 288. We actually found the same result ($\chi_\nu = 1.7$ with $W_0 = 5.8$) for NGC 288 as their result though, we use the result of our calculation and consider NGC 288 is a low concentration cluster. This is since we found the concentration for NGC 288 is $c = 1.0$ for $W_0 = 5.0$ that provides $\chi_\nu = 0.48$ which is smaller than their value $\chi_\nu = 1.7$ with $W_0 = 5.8$ and close to unity.

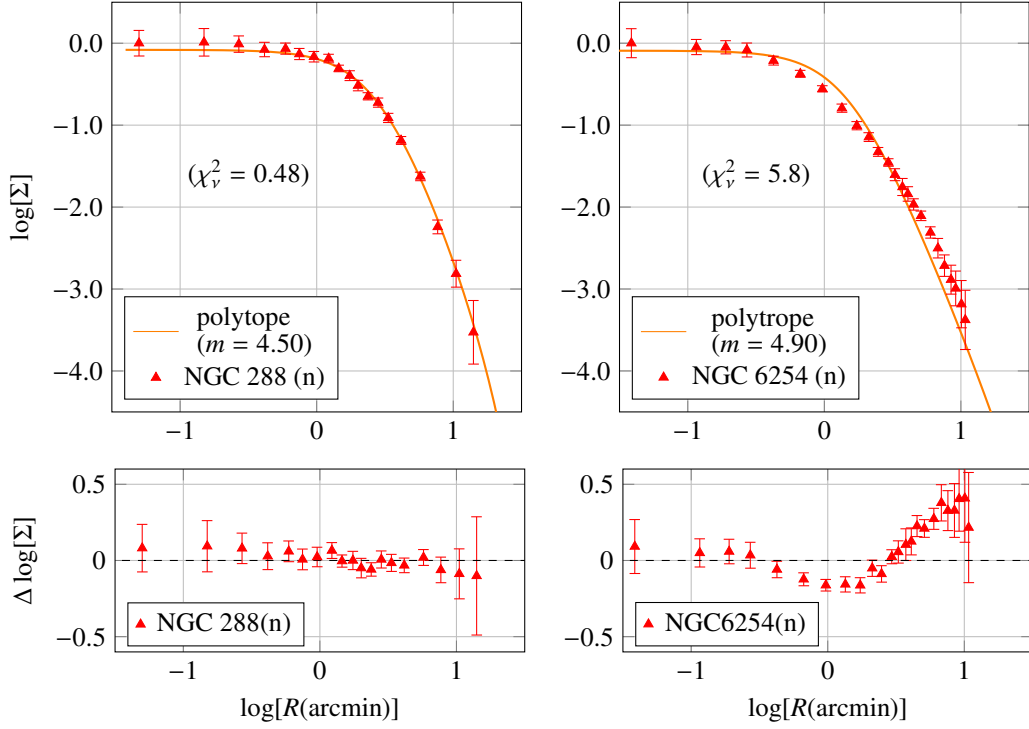


Figure 15: Fitting of the polytropic sphere of index m to the projected density Σ of NGC 288 and NGC 6254 reported in (Mocchi et al., 2013). The unit of Σ is number per square of arcminutes and Σ is normalized so that the density is unity at smallest radius for data. In the legends, (n) means 'normal' or KM cluster as judged so in (Djorgovski and King, 1986). $\Delta \log[\Sigma]$ is the corresponding deviation of Σ from the model.

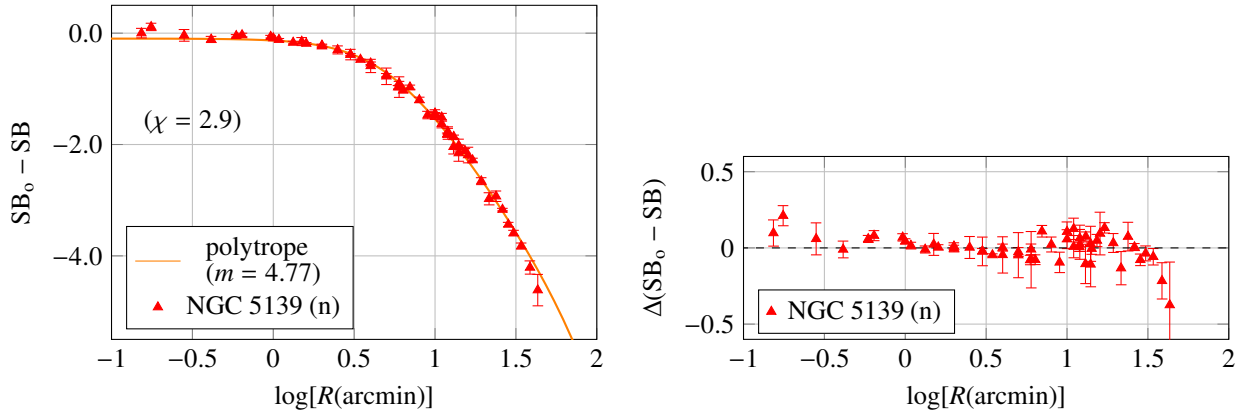


Figure 16: Fitting of the polytropic sphere of index m to the surface brightness of NGC 5139 from (Meylan, 1987). The unit of the surface brightness (SB) is V magnitude per square of arcminutes. The brightness is normalized by the magnitude SB_0 at the smallest radius point. In the legends, (n) means 'normal' or KM cluster as judged so in (Djorgovski and King, 1986). $\Delta(SB_0 - SB)$ is the corresponding deviation of $SB_0 - SB$ from the model.

5.3.1. Discussion of low-concentration clusters being polytropic stellar polytrope

The low-concentration clusters may have cores that are in states of non-equilibrium, possibly modeled by polytropic spheres, rather than a state of (local) thermodynamical equilibrium, if the mass loss from the clusters is less significant. Considering that the King- and energy-truncated-ss-OAFP- models also fit the projected structural profiles of low-concentration globular clusters, the cores of such clusters are apparently well relaxed. Yet, it is not clear

whether their DFs actually have reached a local Maxwellian DF considering that their core relaxation times $t_{c,r}$ are long ($1 \gtrsim \text{Gyr}$) and even the self-similar solution to the OAFP equation can not strictly reach a Maxwellian DF as shown in (Ito, 2020b).

In the initial stage of relaxation evolution in globular clusters, the relaxation process may be dominated by its non-dominant effect on order of secular evolution time scale $t_{\text{sec}} \sim N t_{\text{cross}}$ where t_{cross} is the crossing time. The scale of half-mass relaxation time $t_r/t_{\text{cross}} \sim N/\ln[N]$ is the case when stars can orbit at possible maximum apocenter that is the tidal radius r_{tid} and minimum pericenter that is order of r_{tid}/N . Yet, in the early stage of evolution the pericenter may be much larger on average. The extreme cases were discussed and mathematical formulated in (Kandrup, 1981, 1988). When stars are enough far from each other, ideally many of them separate from the others at order of $1/n^{1/3} \sim r_{\text{tid}}$. The dominant effect discussed in (Chandrasekhar, 1943), that corresponds with order of stellar separation from r_{tid}/N up to $1/n^{1/3}$, may not be important and (non-dominant) many-body effect can be more effective. For homogeneous self-gravitating systems, we can directly use the (local) relaxation time as the measure of relaxation, while in case of inhomogenous system we also need to consider the non-dominant (many-body relaxation) effect which is effective on time scales longer than $t_{c,r}$ by a factor of $\sim \ln[0.1N]$. The mathematical formulation including many-body effect for relaxation time is no longer logarithmic but it mitigates in collision integral as summation of Fourier series expansion under orbit-averaging of kinetic equation (Polyachenko and Shukhman, 1982; Ito, 2018) and order of the many-body relaxation time is $\sim N t_{\text{cross}}$ rather than $N/\ln[N] t_{\text{cross}}$ in the early stage. Kandrup (1985) discussed some simple examples for this matter by neglecting the effect of evaporation and gravothermal instability, which is the case when the two-body relaxation processes are not dominant yet. To avoid evaporation, Kandrup (1985) considered the self-gravitating system is confined in a box and discussed a secular evolution by terming relaxation process 'anomalous' collision that may cause a deviation of stellar DF from Maxwellian DF on the secular evolution time scale.

Table 3 shows the time-scales of dynamics; current and estimated initial relaxation times $t_{c,r}$ and $t_{c,r,0}$ and age t_{age} of clusters with the total mass M . We estimated the values of $t_{c,r,0}$ using the analysis of (Lightman, 1982). Here what we would like to know is how many initial secular evolution times have already passed during their cluster ages. This may be measured by the following 'secular-evolution' parameter

$$\eta_M \equiv \frac{t_{\text{age}}}{t_{\text{sec}}}, \quad (5.2)$$

where the secular evolution time is defined as

$$t_{\text{sec}} \equiv \ln \left[0.11 \frac{M}{M_\odot} \right] t_{c,r,0}, \quad (5.3)$$

where M_\odot is the solar mass and M the dynamical mass for each cluster reported in (Mandushev et al., 1991). The natural log and factor 0.11 are introduced so that the mathematical expression for $t_{c,r,0}$ follows the core relaxation time of (Spitzer, 1988) and quantitatively the results of N -body simulations (Aarseth and Heggie, 1998). In (Lightman, 1982) to calculate the completion rate, the initial relaxation time $t_{c,r,0}$ was compared to the order of cluster age $t_{o,\text{age}}$ while we would like to compare t_{sec} and t_{age} to see whether the clusters could have reached a state described by (local) Maxwellian DF in their cores. If $\eta_M \gtrsim 1$, the core of a cluster may be a state described by Maxwellian DF while if $\eta_M \lesssim 1$ the cluster may be in a non-equilibrium state at present; the latter would provide some insight of polytropic model being a possible model for low-concentration clusters. Table 3 shows that the globular clusters well fitted by polytropic spheres have small η_M ($0.20 < \eta_M \lesssim 1$). On one hand, the parameter η_M of the clusters that could not be fitted by polytropes are $1 \lesssim \eta_M \lesssim 3.77$ on which the maximum value was achieved by NGC 7099 (one of PCC clusters). NGC 3201 and NGC 4590 are classified into the intermediate class in which a polytropic model is apparently fitted to the projected structural profiles at part of cluster radii. Figure 17 shows the secular evolution rate against concentration c ; for the concentration we employed the (Harris, 1996, (2010 edition))'s values. It appears that $\eta_M = 1$ is a good threshold to separate polytropic- and non-polytropic clusters. Especially when $c \approx 1.5$ and $\eta_M \approx 1$, both the polytropic- and non-polytropic clusters coexist.

The realization of polytropic clusters was discussed by (Taruya and Sakagami, 2003) based on N -body simulation. Assuming a self-gravitating system of equal-mass is enclosed in an adiabatic container, they found the simulated distribution function can be well approximated by stellar polytropes even on time scales much longer than half-mass relaxation time. This was also confirmed using isotropic time-dependent Fokker-Planck model (Taruya and Sakagami,

2004). Especially, Taruya and Sakagami (2003) also tested the system without an adiabatic wall; of course, due to the evaporation stellar DF largely deviates from the stellar polytrope while in the early stage of evolution the simulated DF seems well fitted by the DF for polytropes; in their work $m = 5.7$ at $T = 50$ seems provide a DF reasonably close to the DF for a polytrope. Also, the inner part of the systems and stellar DF at low energy are well fitted by DF for polytropes regardless of the effect of escaping stars. Their results implicates that the stellar DF and structural profile of star cluster can be alike a polytrope unless the effect of evaporation is dominant.

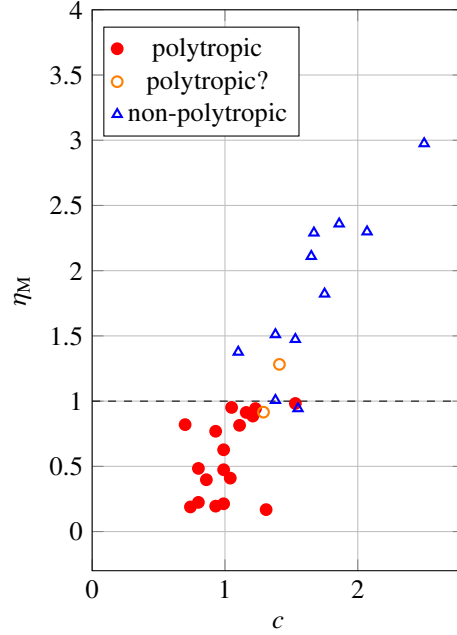


Figure 17: Secular relaxation parameter η_M against concentration c . The values of concentration are adapted from (Harris, 1996, (2010 edition)).

5.3.2. Criticism on polytropic globular clusters

The discussion for polytropic globular clusters in Section 5.3.1 is oversimplified in the sense that actual globular clusters are subject to mass spectrum (segregation) with stellar evolution and tidal effects (shock), hence the clusters are supposed to have lost a significant amount of stars while the relation of mass spectrum and polytrope sphere has not been discussed, which indicates polytropic globular clusters are a phenomenological concept. In the case of *isolated* N -body system with *equal* mass, the cluster loses a small fraction ($\sim 0.1\%$) of total stellar mass in the first five initial relaxation time scale (Baumgardt et al., 2002). Yet, more realistically mass segregation and tidal effect in general make faster the process leading to core collapse (Spitzer, 1988; Binney and Tremaine, 2011) which was originally discussed for both multi-mass OAFP model (e.g. Chernoff and Weinberg, 1990; Takahashi and Lee, 2000) and N -body simulation (e.g. Fukushige and Heggie, 1996; Portegies Zwart et al., 1998; Baumgardt and Makino, 2003) in tidal field. Especially, relatively-new observation showed an unexpected feature of low-concentration clusters; the clusters have depleted mass functions of low-mass stars compared to high-concentration ones (Marchi et al., 2007). This result means that the lower-concentration clusters have lost more stars due to evaporation or tidal stripping, which was caused by mass segregation through two-body relaxation and tidal effect from the Galaxy. The excessive loss of low-mass stars from low-concentration clusters contradicts standard stellar dynamics in which higher-concentration clusters are supposed to have lost more low-mass stars due to more frequent two-body relaxation process. Based on direct N -body simulation, (Baumgardt et al., 2008) explained one possible interpretation for this issue by showing that the low-concentration clusters had already undergone primordial mass segregation in the early stage of evolution due to stellar evolution. This idea was extended to a sophisticated case study for one of low-concentration clusters, Palomar 4 (Zonoozi et al., 2017); the total mass rapidly decreases only in the first 0.1 Gyr and the mass of the cluster calmly keeps decreasing. The decrease in mass depends on the orbit of Palomar 4 though, star's total number decreases in 10

polytropic cluster	c	$t_{c.r.}$ (Gyr)	$t_{c.r.o}$ (Gyr)	$\log\left[\frac{M}{M_{\odot}}\right]$	η_M	t_{age} (Gyr)	Reference for t_{age}
NGC 288	0.99	0.98	2.0	4.64	0.63	10.62	(Forbes and Bridges, 2010)
NGC 1261	1.16	0.39	1.15	5.17	0.913	10.24	(Forbes and Bridges, 2010)
NGC 5053	0.74	6.5	8.2	4.41	0.19	12.29	(Forbes and Bridges, 2010)
NGC 5139	1.31	4.0	5.5	6.38	0.17	11.52	(Forbes and Bridges, 2010)
NGC 5466	1.04	2.2	3.6	4.85	0.41	13.57	(Forbes and Bridges, 2010)
NGC 5897	0.86	2.1	3.5	4.83	0.40	12.3	(Forbes and Bridges, 2010)
NGC 5986	1.23	0.38	1.24	5.48	0.94	12.16	(Forbes and Bridges, 2010)
NGC 6101	0.80	1.6	2.9	4.83	0.48	12.54	(Forbes and Bridges, 2010)
NGC 6205	1.53	0.32	1.12	5.59	0.98	11.65	(Forbes and Bridges, 2010)
NGC 6402	0.99	1.14	2.35	5.89	0.47	12.6	(Santos and Piatti, 2004)
NGC 6496	0.70	0.87	2.0	4.29	0.82	12.42	(Forbes and Bridges, 2010)
NGC 6712	1.05	0.40	1.2	4.98	0.95	10.4	(Forbes and Bridges, 2010)
NGC 6723	1.11	0.62	1.7	5.15	0.81	13.06	(Forbes and Bridges, 2010)
NGC 6809	0.93	0.72	1.8	5.03	0.77	13.0±0.3	(Wang et al., 2016)
NGC 6981	1.21	0.52	1.4	4.80	0.89	10.88	(Forbes and Bridges, 2010)
Pal 3	0.99	4.5	5.8	4.36	0.21	9.7	(Forbes and Bridges, 2010)
Pal 4	0.93	5.2	6.5	4.21	0.19	9.5	(Forbes and Bridges, 2010)
Pal 14	0.80	7.1	8.6	3.83	0.22	13.2 ± 0.3	(Sollima et al., 2010)

polytropic cluster?	c	$t_{c.r.}$ (Gyr)	$t_{c.r.o}$ (Gyr)	$\log\left[\frac{M}{M_{\odot}}\right]$	η_M	t_{age} (Gyr)	Reference for t_{age}
NGC 3201	1.29	0.41	1.2	5.05	0.92	10.24	(Forbes and Bridges, 2010)
NGC 4590	1.41	0.28	1.1	4.95	1.29	13.0 ± 1.0	(Dotter et al., 2009)

non-polytropic cluster	c	$t_{c.r.}$ (Gyr)	$t_{c.r.o}$ (Gyr)	$\log\left[\frac{M}{M_{\odot}}\right]$	η_M	t_{age} (Gyr)	Reference for t_{age}
NGC 1851	1.86	0.027	0.38	5.42	2.36	9.2±1.1	(Salaris and Weiss, 2002)
NGC 5634	2.07	0.047	0.53	5.18	2.30	11.8	(Forbes and Bridges, 2010)
NGC 6121	1.65	0.079	0.61	4.83	2.11	11.5±0.4	(Wang et al., 2016)
NGC 6144	1.55	0.60	1.7	4.76	0.94	13.82	(Forbes and Bridges, 2010)
NGC 6254	1.38	0.16	0.81	5.06	1.51	11.39±1.1	(Forbes and Bridges, 2010)
NGC 6273	1.53	0.33	1.1	6.03	1.47	11.90	(Forbes and Bridges, 2010)
NGC 6352	1.10	0.29	1.1	4.57	1.37	12.67	(Forbes and Bridges, 2010)
NGC 6388	1.75	0.052	0.553	6.16	1.82	12.03	(Forbes and Bridges, 2010)
NGC 6626	1.67	0.042	0.52	5.36	2.29	12.1±1.0	(Kerber et al., 2018)DSED method
NGC 6656	1.38	0.34	1.2	5.53	1.00	12.67	(Forbes and Bridges, 2010)
NGC 7099(c)	2.50	0.0023	0.35	4.91	2.97	12.93	(Forbes and Bridges, 2010)

Table 3: Secular parameters calculated from the core relaxation times and ages of polytropic- and non-polytropic- clusters. The current relaxation time $t_{c.r.}$ and concentration c are values reported in (Harris, 1996, (2010 edition)). The total masses $\log\left[\frac{M}{M_{\odot}}\right]$ are from (Mandushev et al., 1991) where M_{\odot} is solar mass. We adapted the ages of clusters from (Forbes and Bridges, 2010) and we resorted to other sources when we found more recent data or could not find the cluster age in (Forbes and Bridges, 2010).

Gyr by approximately 60 %. It appears that the reason why the low-concentration clusters have polytropic structures is not directly due to little loss of stars. Hence, one needs to directly discuss the relation of the DF for polytrope and globular clusters that have experienced mass segregation, which has not been detailed.

Also, the present work does not discuss the projected line-of-sight velocity dispersion profiles of the energy-truncated ss-OAFP model. Many of the polytropic clusters are low-concentration clusters, which implicates accurate observational data are hard to be obtained compared to high-concentration clusters (e.g. Meylan and Heggie, 1997). Perhaps, more recent data from *Gaia 2* (e.g. Baumgardt et al., 2018), the ESO Multi-instrument Kinematic Survey (MIKIS) (Ferraro et al., 2018) and more accurate kinematic data may differentiate the King model from the energy-truncated ss-OAFP model.

As a conclusion of the present section, we consider the polytropic globular clusters may 'phenomenologically' apply to the structure of low-concentration clusters in a similar way that the energy truncation for ss-OAFP model based on a polytrope is not endorsed by a strict first principle. Since the discussion is not matured on the relation between mass segregation (spectrum) and stellar DF for polytrope, we need further examine this topic in future with more accurate observed structural- and kinematic- data and realistic numerical simulation. We believe especially the kinematic data can draw a line in applicability between the King and our model.

6. Conclusion

The present work introduced a phenomenological model i.e. the energy-truncated ss-OAFP model that can fit the projected density profiles for at least half of Milky Way globular clusters including PCC clusters with resolved cores, aiming at establishing a model with wide applicability compared to the classical isotropic one-component King model. The present model is a linear algebraic combination of the DFs for the ss-OAFP model and polytropic sphere of m ; the latter was weighted by a factor of δ . The optimal value of m was identified as 3.9 by comparing the concentrations and tidal (limiting) radii of the King- and our models. After this procedure, this new model has only three degrees of freedom that are the same as those of the King model while our model can even fit to the projected structural profiles of PCC clusters with resolved core in addition to those of KM clusters. The fitting results provided a completion rate of core collapse against concentration including PCC clusters with resolved-core that is consistent to standard stellar dynamics. Also, our model is more useful compared to the King model to single out KM clusters whose morphology is close to the core-collapsing cluster i.e. high concentration $\bar{c} \geq 2.0$; examples are NGC 1851, NGC 6626 and NGC 6517.

Our model also can apply to globular clusters in a broad range of radii 0.01 ~ 10 arcminutes with higher $m(\geq 4.2)$, however the energy-truncation based on polytrope provides unrealistically large tidal radius. Hence, we also proposed an approximated form of the energy-truncated ss-OAFP model to avoid unrealistic tidal radii. Lastly, we discussed that the low-concentration globular clusters may be polytropic in the sense that their projected structural profiles are well fitted by those of polytropes. Yet, the physical arguments and previous numerical results for the polytropic globular clusters are not well established. Hence, we consider the polytropic clusters are a heuristic idea for now, which intrigues us to work in future on examining (i) the relation of mass spectrum (segregation) of star clusters and stellar DF for polytropes and (ii) the relation of the low-concentration clusters with stellar polytrope that obeys the generalized statistical mechanics based on Tsallis entropy and (iii) applicability of the King- and our models to kinematic profiles.

Acknowledgements

The present work is partial fulfillment of the degree of Philosophy at CUNY graduate center.

Appendix A Fitting of the finite ss-OAFP model to King-model clusters

The present appendix shows fitting of the energy-truncated ss-OAFP model to projected structural profiles of Galactic KM clusters reported in (Kron et al., 1984; Noyola and Gebhardt, 2006; Miocchi et al., 2013). For fitting

to (Miocchi et al., 2013)'s data we chose the fitting parameters in the model so that χ^2_ν is minimized. For fitting to (Kron et al., 1984; Noyola and Gebhardt, 2006)'s data, the deviation of the model from the data plots are minimized. Section A.1, A.2 and A.3 show fitting of our model to the KM stars reported in (Miocchi et al., 2013), (Kron et al., 1984) and (Noyola and Gebhardt, 2006).

A.1 KM cluster (Miocchi et al., 2013)

Figures A.18, A.19 and A.20 depict the energy-truncated ss-OAFP model fitted to the projected density profiles of KM clusters reported in (Miocchi et al., 2013). Table A.4 compares the structural parameters of our model, King model and Wilson model. Majority of the parameters obtained from our model is greater than those of the King model but less than those of the Wilson model. The energy-truncated ss-OAFP model does not completely fit the structures of NGC 5466 and Terzan 5 while the King- and Wilson- models do fit them, which implies that they are less close to neither of the states of core collapse (or gravothermal instability phase) nor polytropic sphere (possibly collisionless phase).

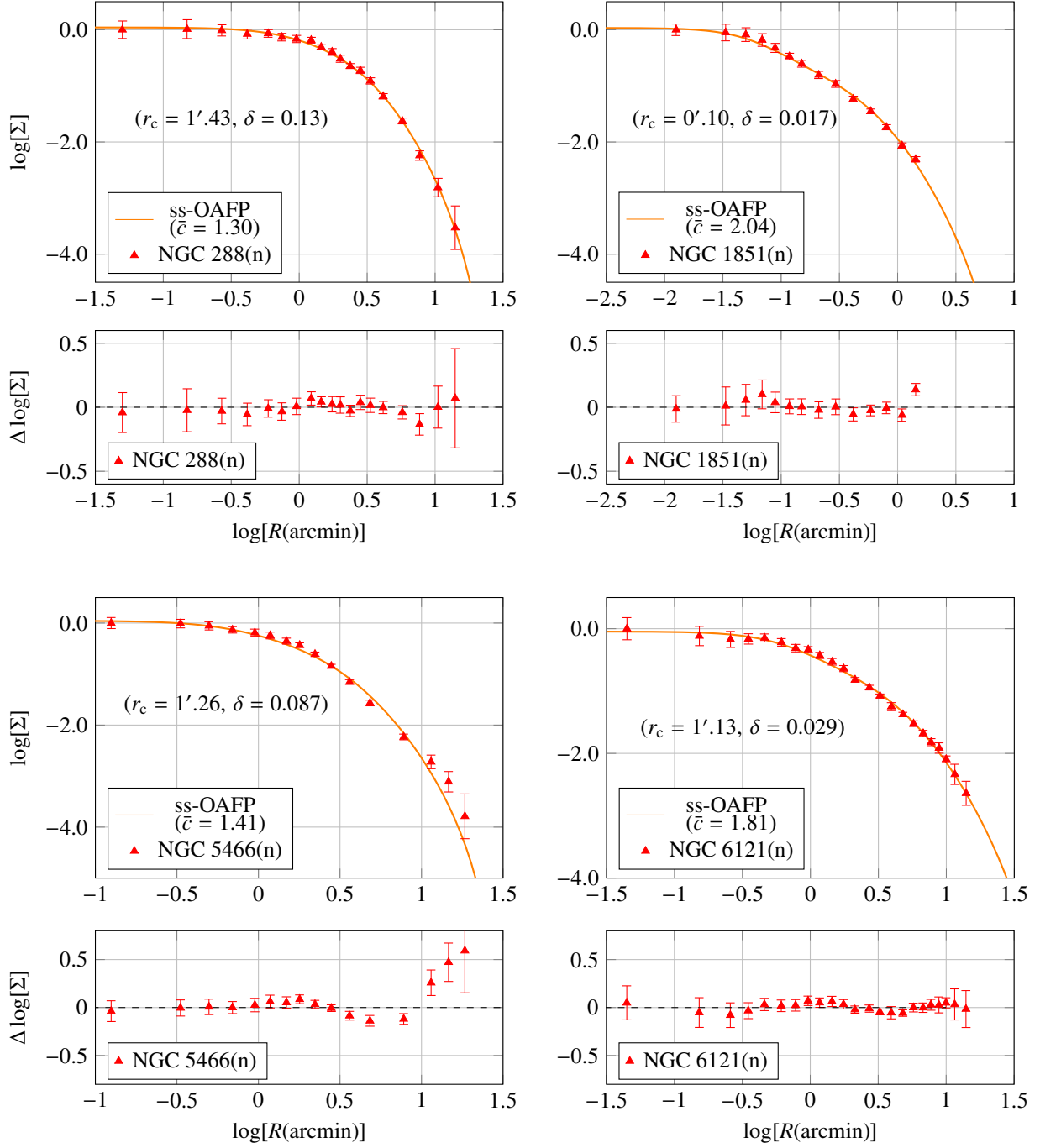


Figure A.18: Fitting of the energy-truncated ss-OAFP model ($m = 3.9$) to the projected density Σ of NGC 288, NGC 1851, NGC 5466 and NGC 6121 reported in from (Miocchi et al., 2013). The unit of Σ is number per square of arcminutes and Σ is normalized so that the density is unity at the smallest radius for data. In the legends, (n) means 'normal' cluster that can be fitted by the King model as judged so in (Djorgovski and King, 1986). $\Delta \log[\Sigma]$ is the corresponding deviation of Σ from the model on log scale.

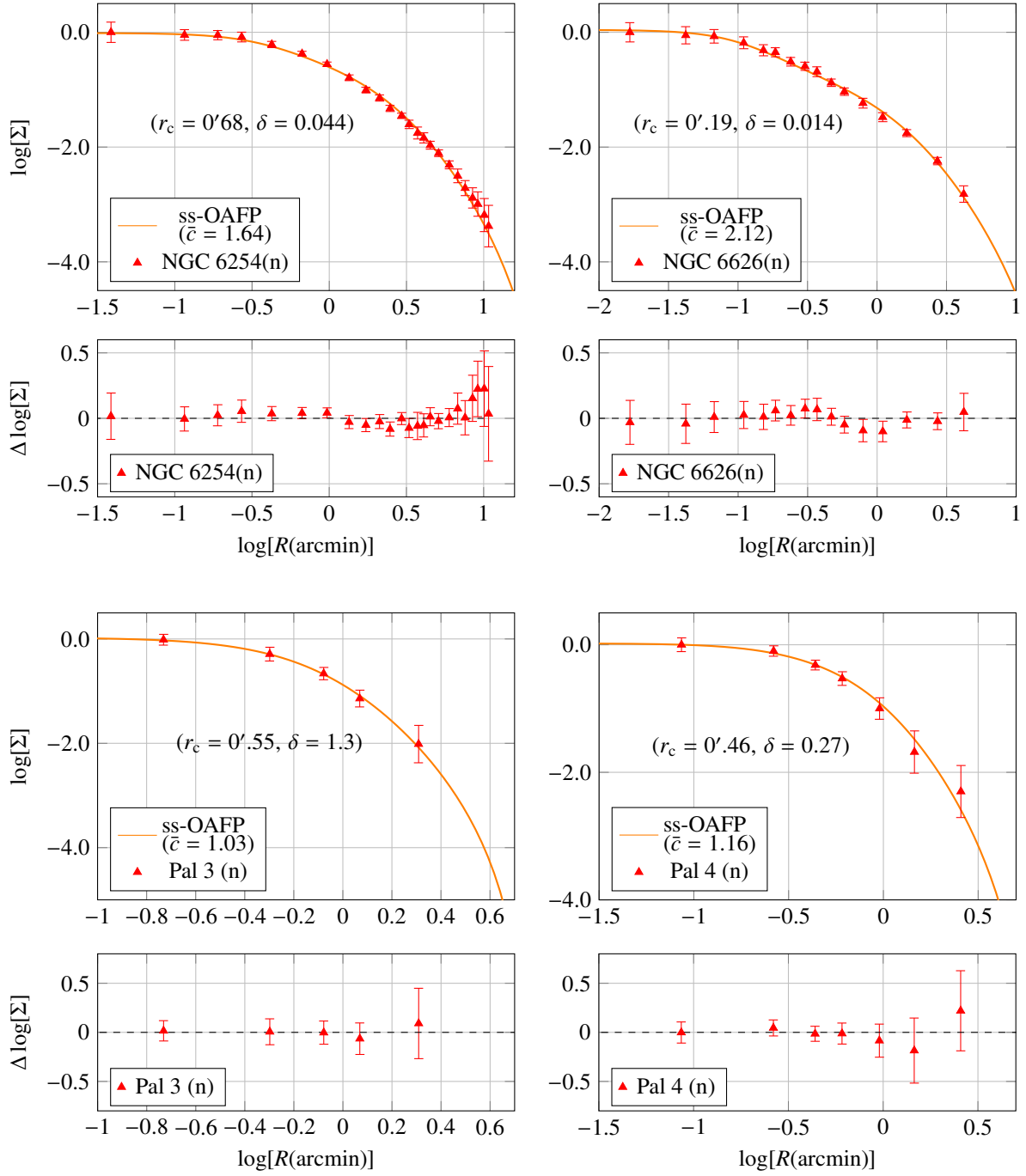


Figure A.19: Fitting of the energy-truncated ss-OAFP model ($m = 3.9$) to the projected density Σ of NGC 6254, NGC 6626, Pal 3 and Pal 4 reported in (Miocchi et al., 2013). The unit of Σ is number per square of arcminutes and Σ is normalized so that the density is unity at the smallest radius for data. In the legends, (n) means 'normal' cluster that can be fitted by the King model as judged so in (Djorgovski and King, 1986). $\Delta \log[\Sigma]$ is the corresponding deviation of Σ from the model on log scale.

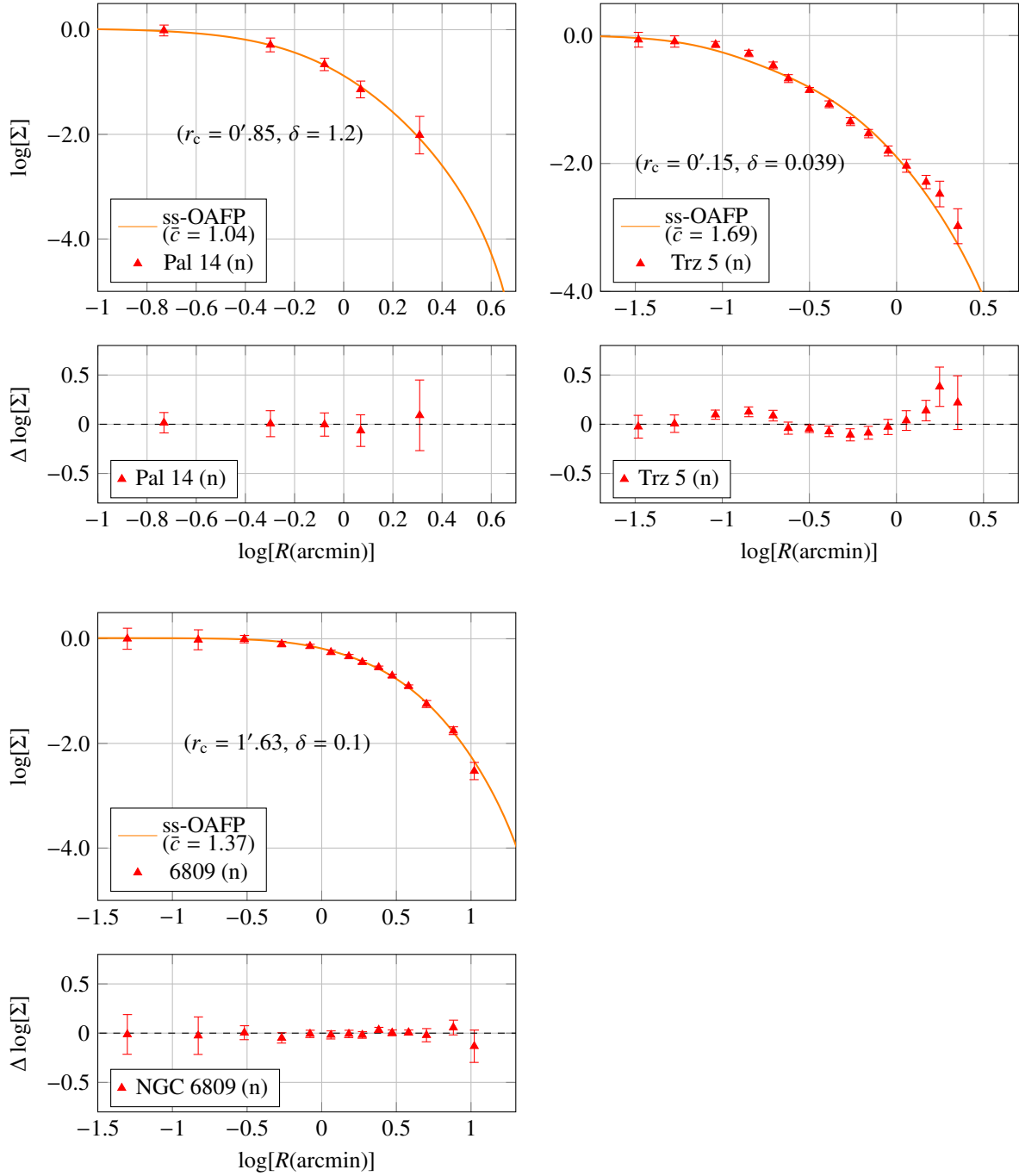


Figure A.20: Fitting of the energy-truncated ss-OAFP model ($m = 3.9$) to the projected density Σ of Palomar 14, Terzan 5 and NGC 6809 reported in (Miocchi et al., 2013). The unit of Σ is number per square of arcminutes and Σ is normalized so that the density is unity at the smallest radius for data. In the legends, (n) means ‘normal’ cluster that can be fitted by the King model as judged so in (Djorgovski and King, 1986). $\Delta \log[\Sigma]$ is the corresponding deviation of Σ from the model on log scale.

A.2 KM clusters (Kron et al., 1984)

Figures A.21- A.24 show the projected density profiles reported in (Kron et al., 1984), fitted by the energy-truncated ss-OAFP model. In (Kron et al., 1984), the first several points are not included in fitting of King model

	NGC 288			NGC 1851			NGC 5466					
	c	r_c	r_{tid}	c	r_c	r_{tid}	c	r_c	r_{tid}			
ss-OAFP model	1.30	1.43	28.9	2.04	0.10	11.1	1.41	1.26	32.4			
King model (Miocchi et al., 2013)	1.20	1.17	21	1.95	0.09	8.3	1.31	1.20	26.3			
Wilson model (Miocchi et al., 2013)	1.10	1.53	25.8	3.33	0.09	204	1.42	1.33	40			
	NGC 6121			NGC 6254			NGC 6626					
	c	r_c	r_{tid}	c	r_c	r_{tid}	c	r_c	r_{tid}			
ss-OAFP model	1.81	1.13	73.6	1.64	0.68	30.1	2.12	0.19	25.4			
King model (Miocchi et al., 2013)	1.68	1.07	53	1.41	0.68	19.0	1.79	0.26	16			
Wilson model (Miocchi et al., 2013)	2.08	1.08	1200	1.80	0.73	52	3.1	0.26	380			
	Pal 3			Pal 4			Pal 14			Trz 5		
	c	r_c	r_{tid}	c	r_c	r_{tid}	c	r_c	r_{tid}	c	r_c	r_{tid}
ss-OAFP model	1.03	0.55	5.91	1.16	0.46	6.79	1.04	0.85	9.23	1.69	0.15	7.25
King model (Miocchi et al., 2013)	0.8	0.47	3.6	1.1	0.37	4.9	0.9	0.68	6.4	1.59	0.13	5.2
Wilson model (Miocchi et al., 2013)	0.81	0.49	5.33	1.3	0.38	9	1.0	0.70	10	2.4	0.14	39

Table A.4: Core- and tidal- radii of finite ss-OAFP model applied to projected density profiles reported in (Miocchi et al., 2013).

due to uncertainty in data originating from too high brightness, yet the present work included them since almost all the data plots were well fitted by our model.

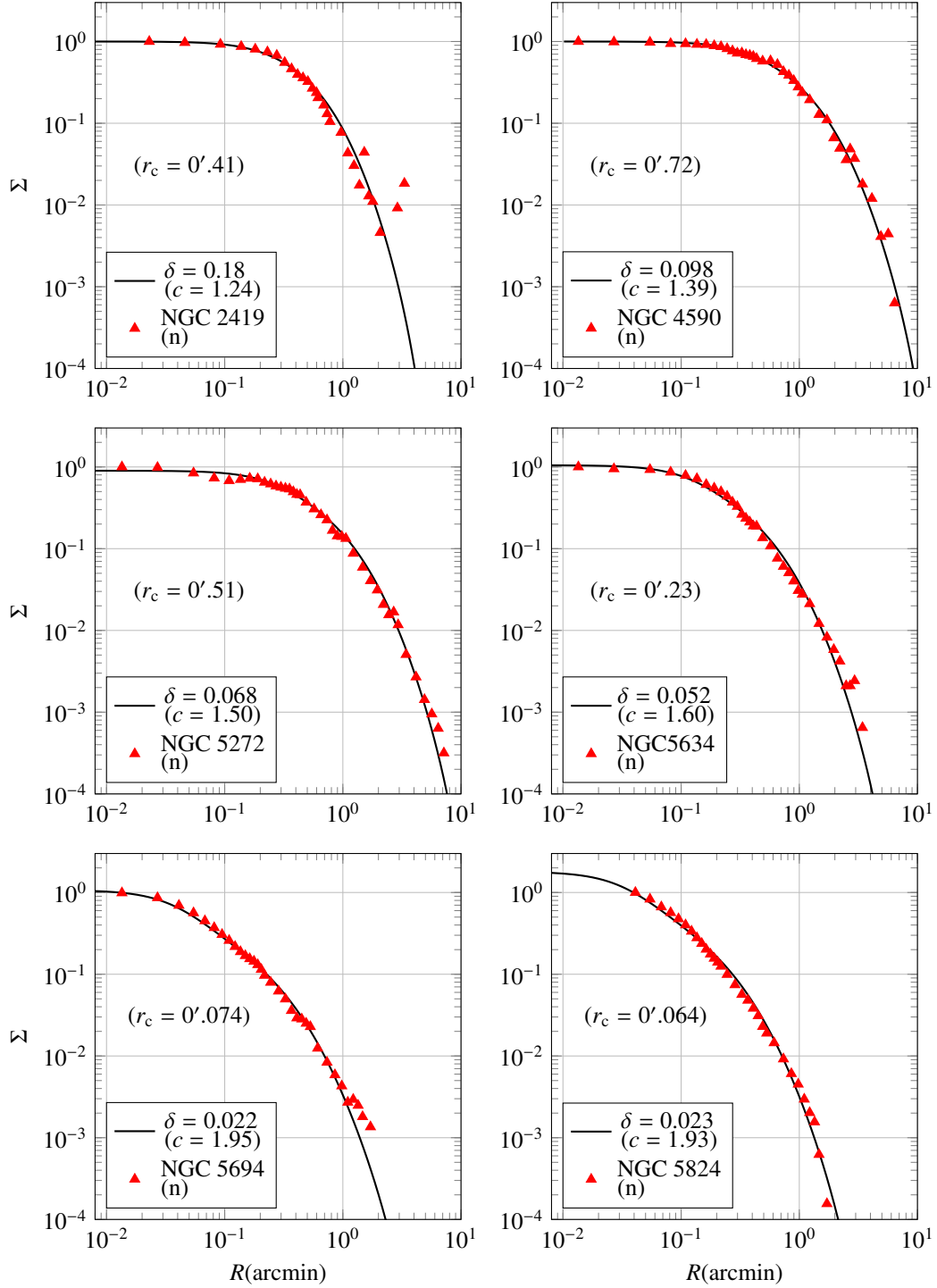


Figure A.21: Fitting of the energy-truncated ss-OAFP model ($m = 3.9$) to the projected density profiles NGC 2419, NGC 4590, NGC 5272, NGC 5634, NGC 5694 and NGC 5824 reported in (Kron et al., 1984). The unit of the projected density Σ is number per square of arcminutes. In the legends, (n) means normal cluster that can be fitted by the King model as judged so in (Djorgovski and King, 1986).

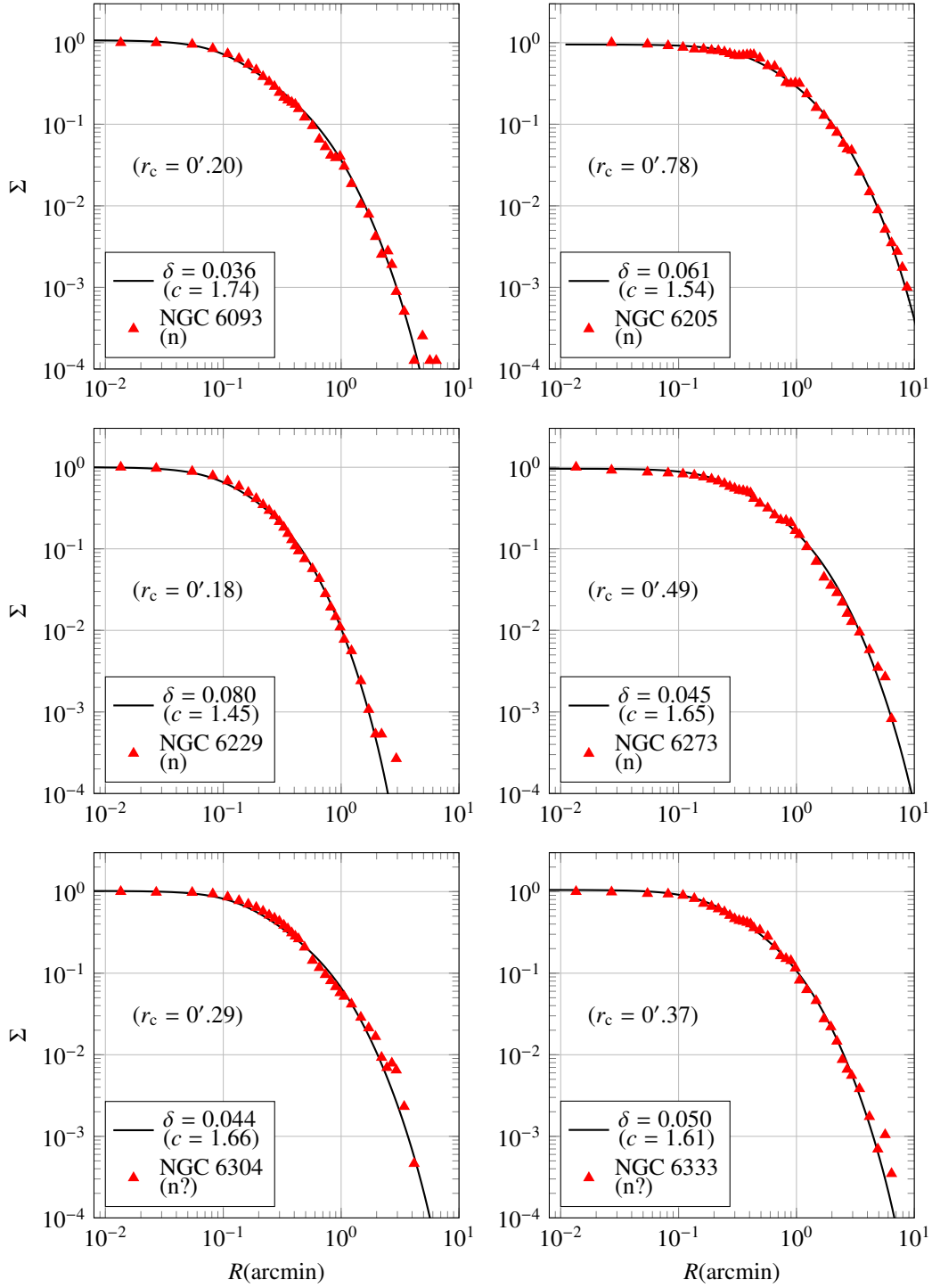


Figure A.22: Fitting of the energy-truncated ss-OAFP model ($m = 3.9$) to the projected density profiles of NGC 6093, NGC 6205, NGC 5229, NGC 6273, NGC 6304 and NGC 6333 reported in (Kron et al., 1984). The unit of the projected density Σ is number per square of arcminutes. In the legends, (n) means ‘normal’ cluster that can be fitted by the King model and (n?) ‘probable normal’ cluster as judged so in (Djorgovski and King, 1986).

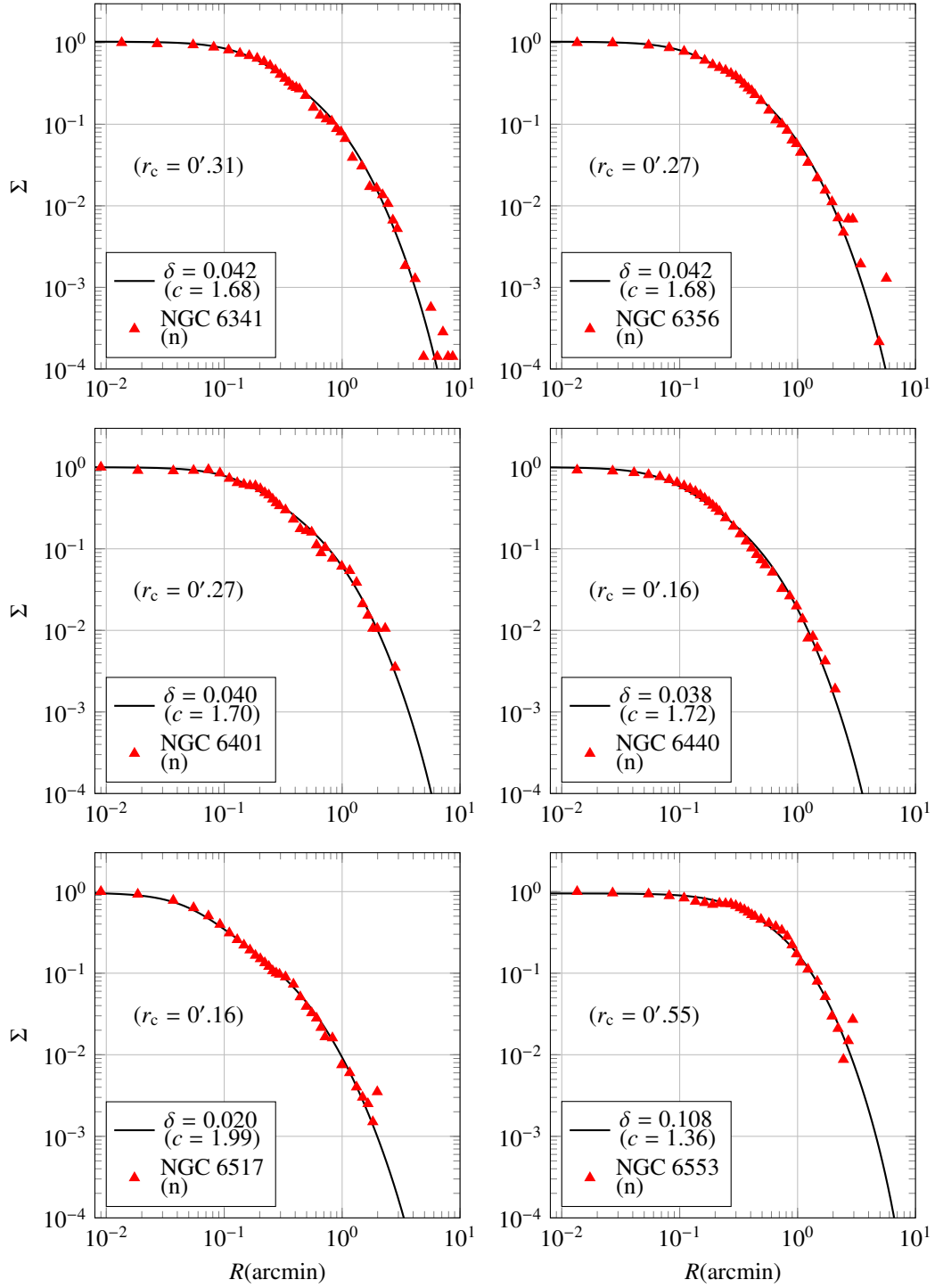


Figure A.23: Fitting of the energy-truncated ss-OAFP model ($m = 3.9$) to the projected density profiles NGC 6341, NGC 6356, NGC 6401, NGC 6440, NGC 6517 and NGC 6553 reported in (Kron et al., 1984). The unit of the projected density Σ is number per square of arcminutes. In the legends, (n) means normal cluster that can be fitted by the King model as judged so in (Djorgovski and King, 1986).

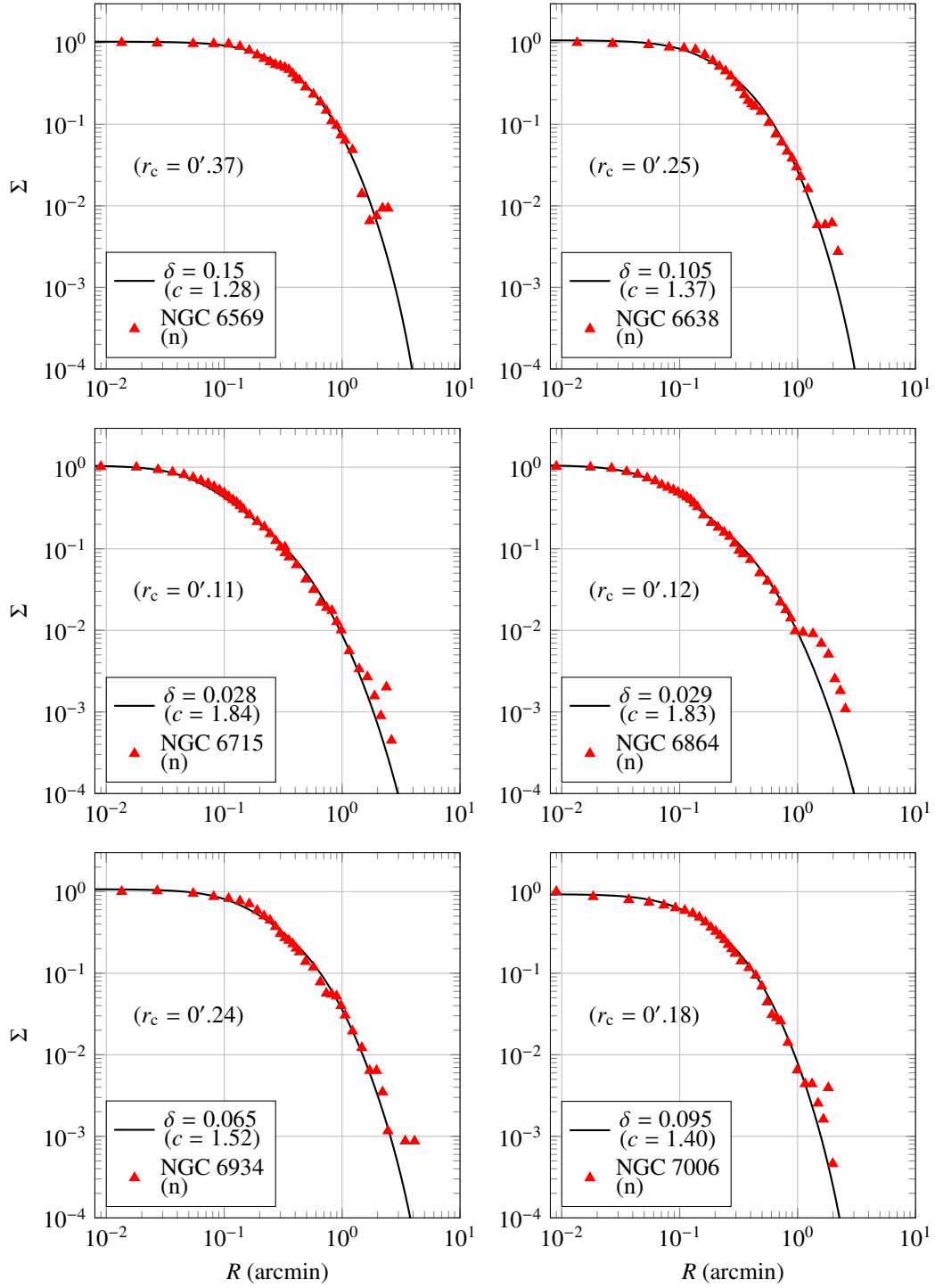


Figure A.24: Fitting of the energy-truncated ss-OAFP model ($m = 3.9$) to the projected density profiles of NGC 6569, NGC 6638, NGC 6715, NGC 6864, NGC 6934 and NGC 7006 reported in (Kron et al., 1984). The unit of the projected density Σ is number per square of arcminutes. In the legends, (n) means normal cluster that can be fitted by the King model as judged so in (Djorgovski and King, 1986).

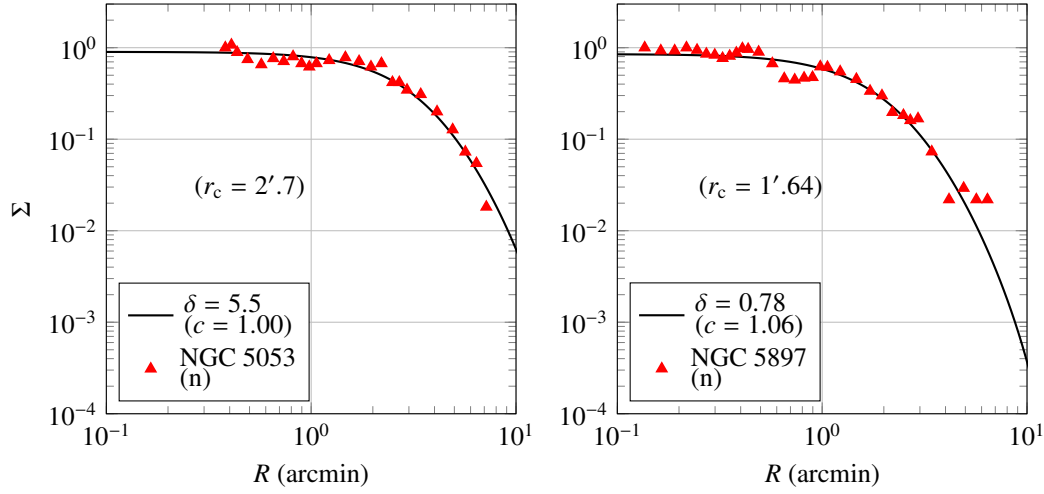


Figure A.25: Fitting of the energy-truncated ss-OAFP model ($m = 3.9$) to the projected density profiles NGC 5053 and NGC 5897 reported in (Kron et al., 1984). The unit of the projected density Σ is number per square of arcminutes. In the legends, (n) means normal cluster that can be fitted by the King model as judged so in (Djorgovski and King, 1986). Following (Kron et al., 1984), data at small radii are ignored due to the depletion of projected density profile.

A.3 KM clusters (Noyola and Gebhardt, 2006)

Figure A.26 shows the fitting of the energy-truncated ss-OAFP model to the surface brightness (V -band magnitude per arcseconds squared) with flat cores reported in (Noyola and Gebhardt, 2006). The brightness is depicted together with the Chebyshev approximation of the brightness reported in (Trager et al., 1995). To fit our model to the profiles, we employed polytropic indices $m = 4.2$ through $m = 4.4$. Figure A.27 depicts the surface brightness profile of globular clusters that our model could not fit due to the cusps in the cores. Figure A.28 depicts the surface brightness profiles fitted by the energy-truncated ss-OAFP model and its approximated model. For approximated models, we needed to employ high polytropic indices $m = 4.8 \sim 4.95$.

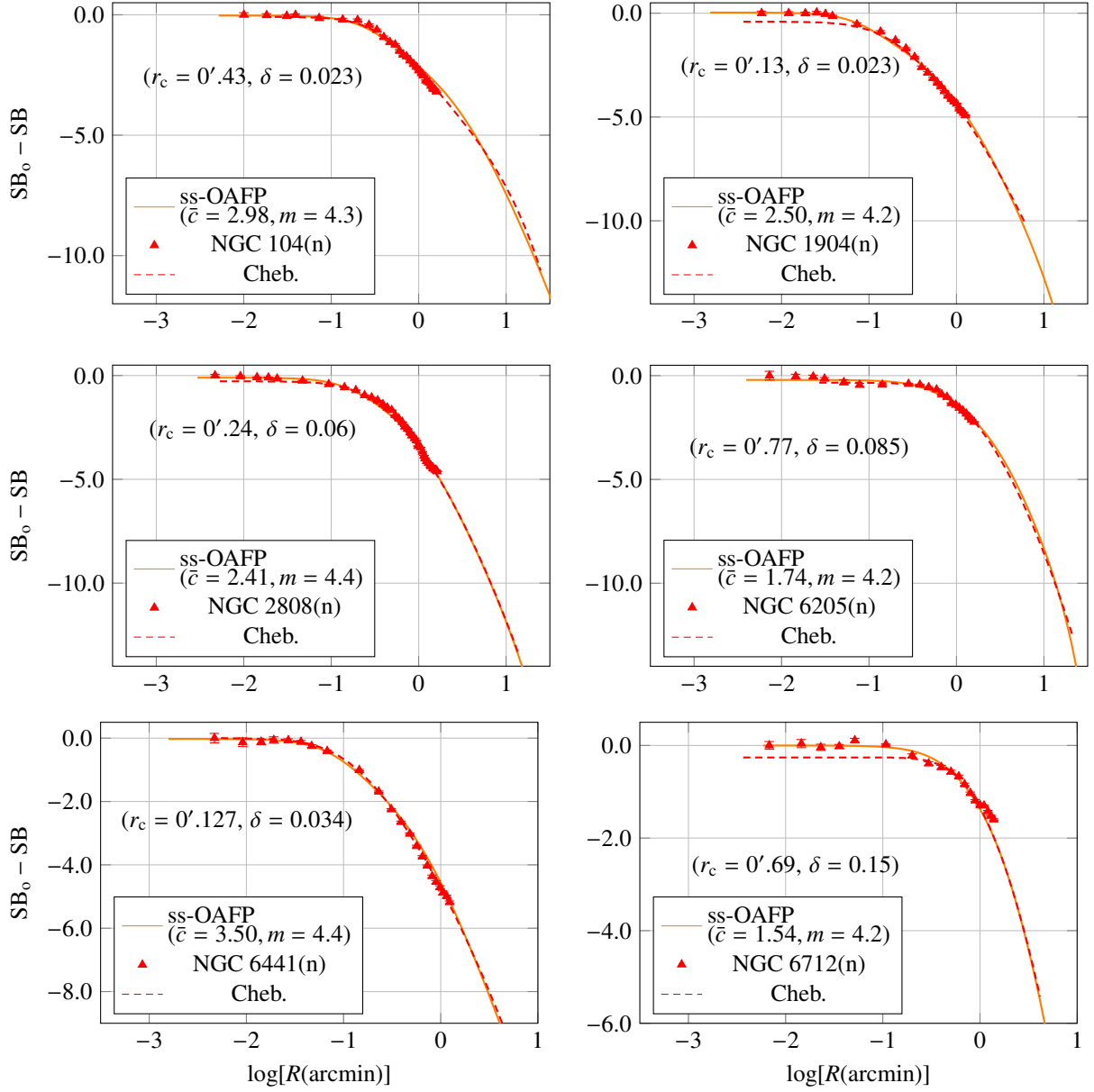


Figure A.26: Fitting of the energy-truncated ss-OAFP model to the surface brightness of NGC 104, NGC 1904, NGC 2808, NGC 6205, NGC 6441, and NGC 6712 reported in (Noyola and Gebhardt, 2006). The unit of the surface brightness (SB) is V magnitude per square of arcseconds. The brightness is normalized by the magnitude SB_0 at the smallest radius point. In the legends, ‘Cheb.’ means the Chebyshev approximation of the surface brightness reported in (Trager et al., 1995) and ‘(n)’ means KM cluster as judged so in (Djorgovski and King, 1986).

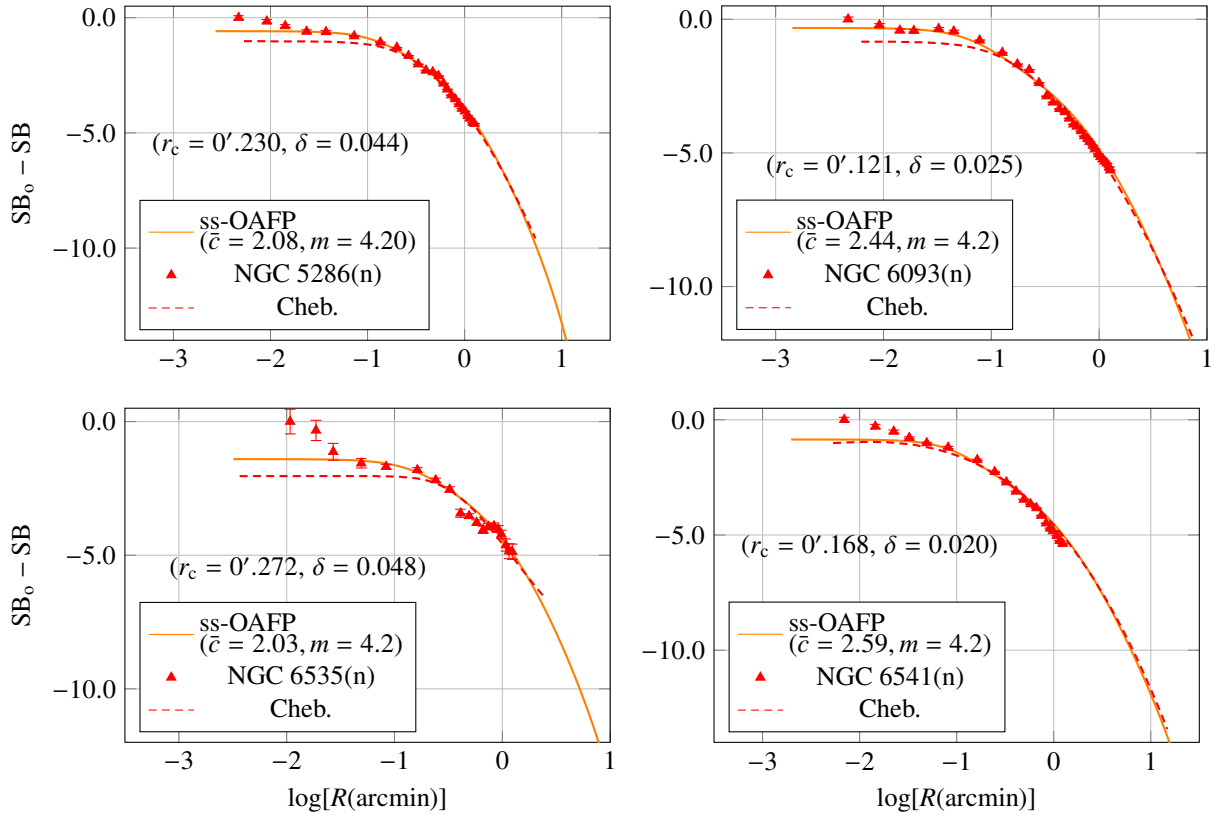


Figure A.27: Failure of fitting of the energy-truncated ss-OAFP model to the surface brightness profiles of NGC 5286, NGC 6093, NGC 6535 and NGC 6541 reported in (Noyola and Gebhardt, 2006). The unit of the surface brightness (SB) is V magnitude per square of arcseconds. The brightness is normalized by the magnitude SB_0 at the smallest radius point. In the legends, 'Cheb.' means the Chebyshev approximation of the surface brightness reported in (Trager et al., 1995) and '(n)' means KM cluster as judged so in (Djorgovski and King, 1986).

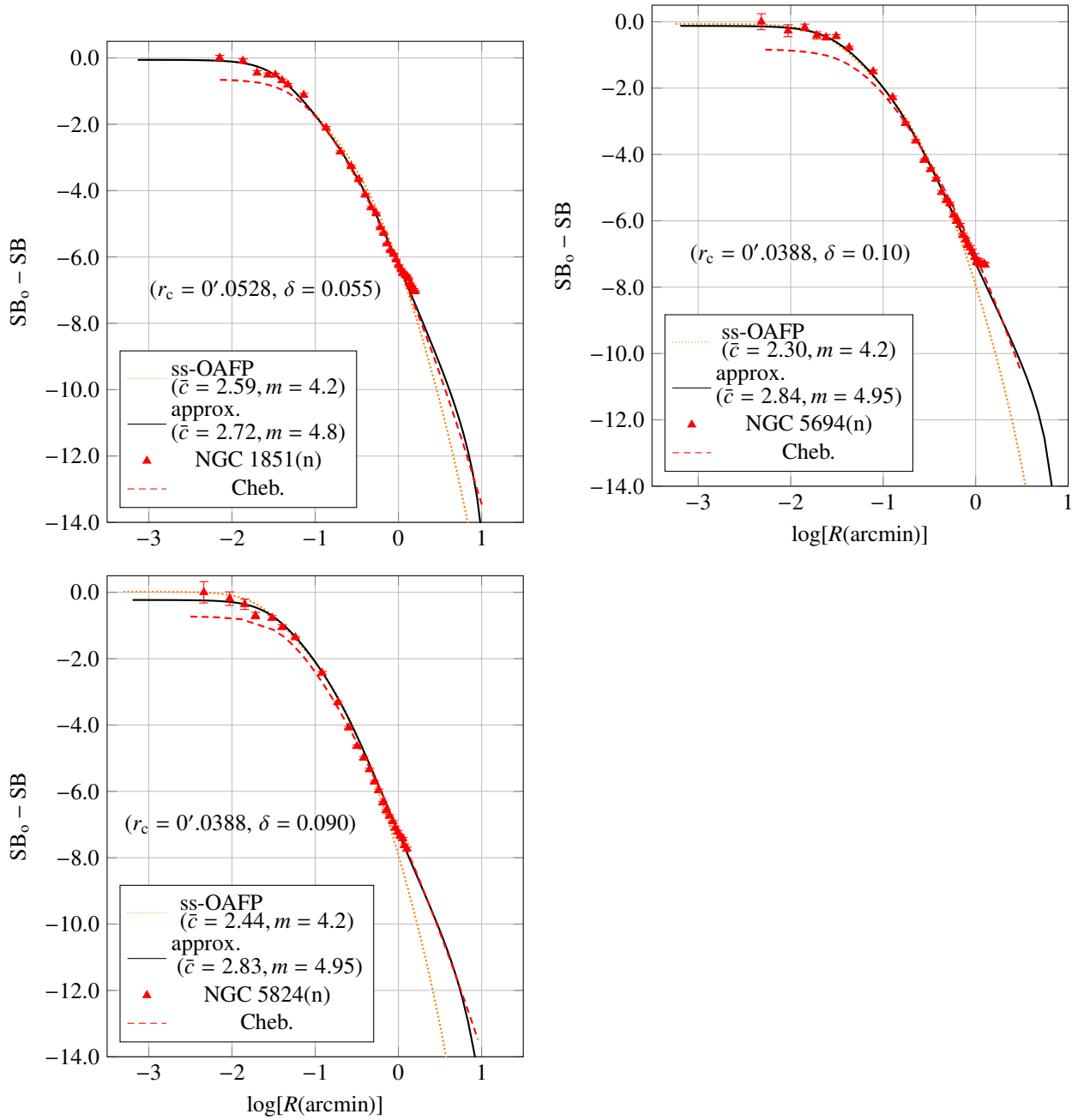


Figure A.28: Fitting of the energy-truncated ss-OAFP model and its approximated form to the surface brightness profiles of NGC 1851, NGC 5694 and NGC 5824 reported in (Noyola and Gebhardt, 2006). The unit of the surface brightness (SB) is V magnitude per square of arcseconds. The brightness is normalized by the magnitude SB_0 at the smallest radius point. The values of r_c and δ were obtained from the approximated form. In the legends, ‘Cheb.’ means the Chebyshev approximation of the surface brightness reported in (Trager et al., 1995) and ‘(n)’ means KM cluster as judged so in (Djorgovski and King, 1986).

Appendix B Fitting of the polytropic sphere model to low-concentration clusters

The present appendix shows the results of application of the energy-truncated ss-OAFP model to PCC clusters reported in (Kron et al., 1984; Lugger et al., 1995; Noyola and Gebhardt, 2006). For fitting of the model to (Kron et al., 1984; Lugger et al., 1995)’s data, the infinite norm of the deviations of the model from the data is minimized while

for fitting to (Lugger et al., 1995), χ^2_ν -value is minimized. Sections B.1, B.2 and B.3 show the fitting to PCC clusters reported in (Kron et al., 1984), (Lugger et al., 1995) and (Noyola and Gebhardt, 2006).

B.1 PCC? clusters (Kron et al., 1984)

Figure B.29 depicts the energy-truncated ss-OAFP model with $m = 3.9$ fitted to the projected density profiles of possible PCC clusters reported in (Kron et al., 1984) in which NGC 1904, NGC 4147, NGC 6544 and NGC 6652 are considered possibly PCC as described in (Djorgovski and King, 1986) by ‘probable/possible’ PCC clusters or ‘the weak indications of PCC’ clusters.

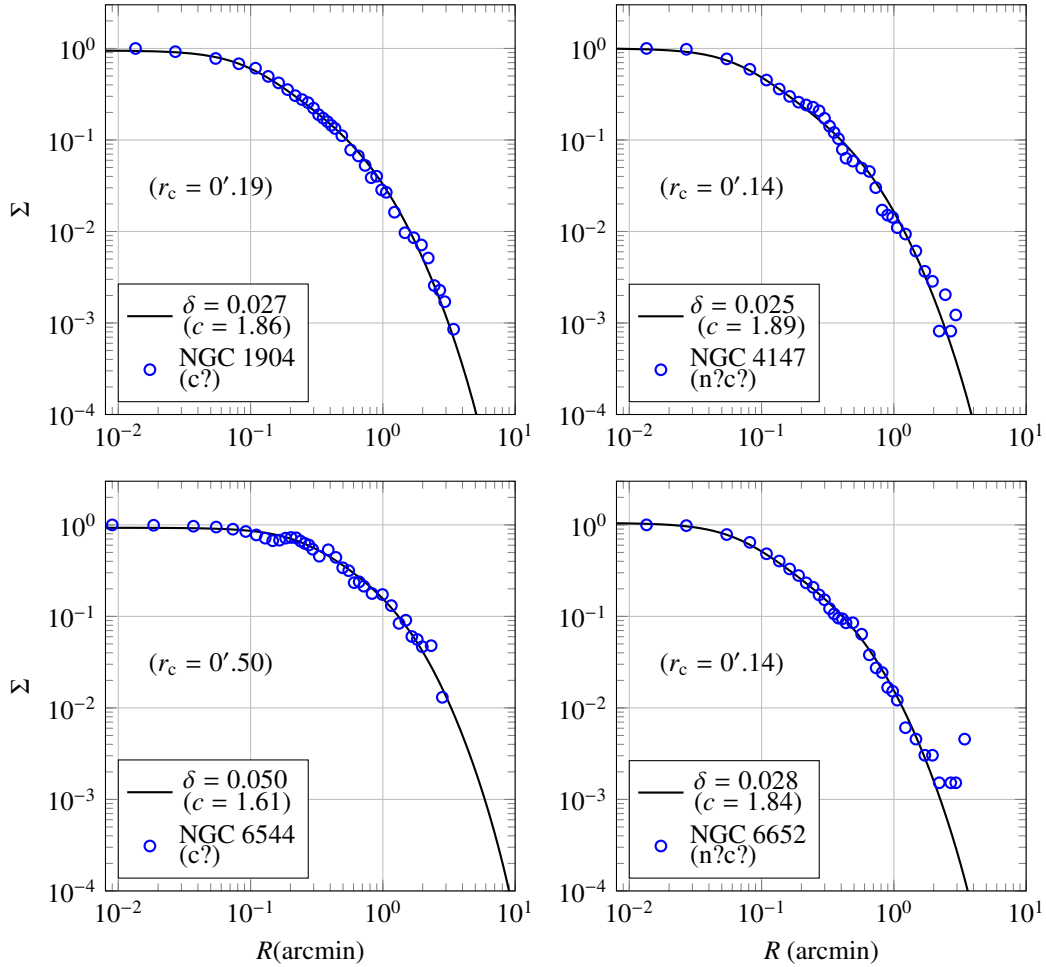


Figure B.29: Fitting of the energy-truncated ss-OAFP model to the projected densities of NGC 1904, NGC 4147, NGC 6544 and NGC 6652 reported in (Kron et al., 1984). The unit of the projected density Σ is number per square of arcminutes. In the legends, (c) means PCC cluster, (c?) probable/possible PCC and (n?c?) weak indications of PCC as judged so in (Djorgovski and King, 1986).

B.2 PCC clusters (Lugger et al., 1995) and (Djorgovski and King, 1986)

Figures B.30 and B.31 show the results of fitting of energy-truncated ss-OAFP model with $m = 3.9$ to the surface brightness profiles of PCC clusters reported in (Lugger et al., 1995) and Terzan 1 in (Djorgovski and King, 1986). For clusters with resolved cores, our model well fits the core and halo at up to 1 arcminute. On one hand, as expected the fitting of our model to the clusters with unresolved core (NGC 5946 and NGC 6624) is not satisfactory while NGC 6342 is one of them but appears reasonably fitted by our model.

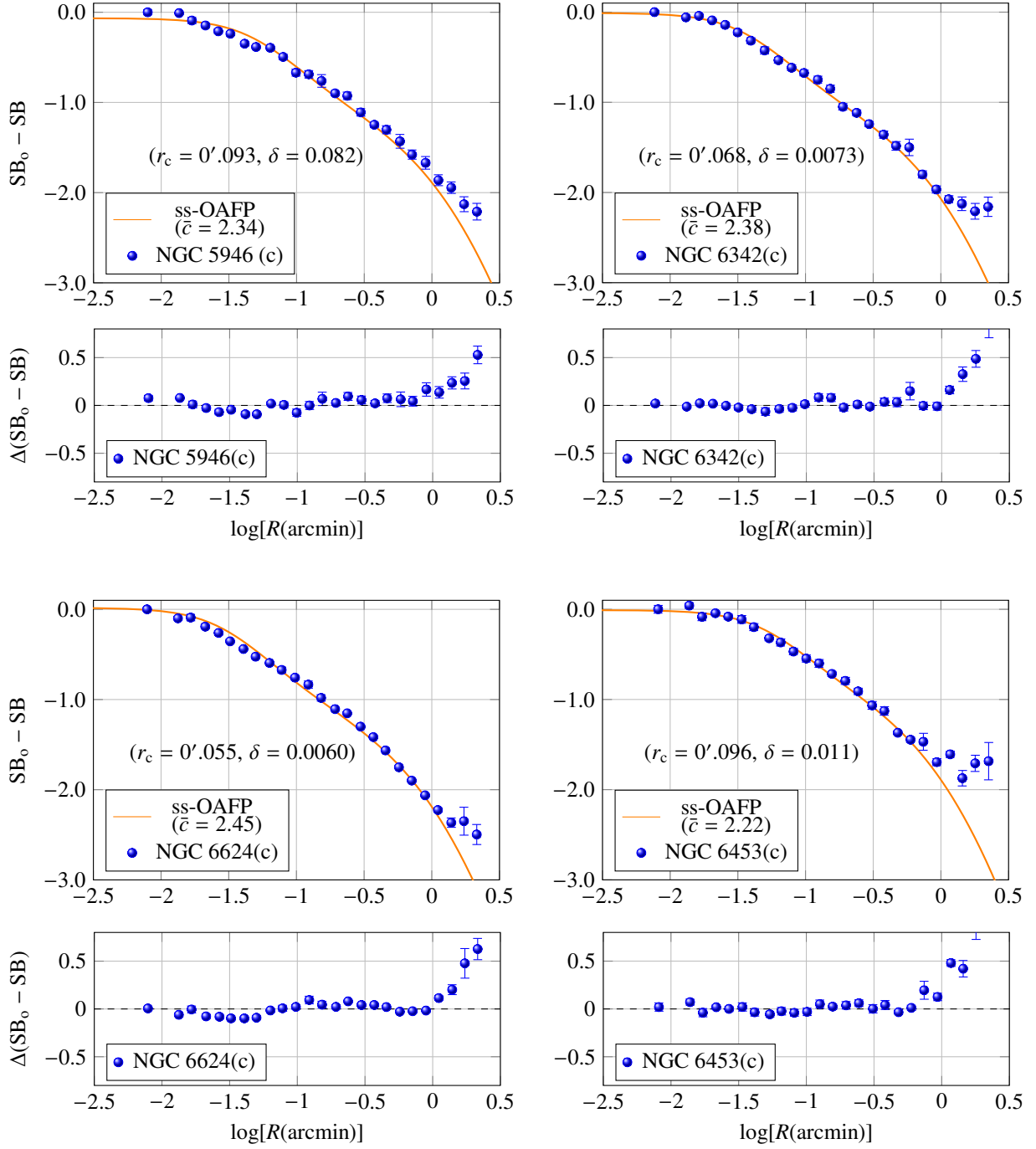


Figure B.30: Fitting of the energy-truncated ss-OAFP model to the surface brightness profiles of NGC 5946, NGC 6342, NGC 6624 and NGC 6453 reported in (Lugger et al., 1995). The unit of the surface brightness (SB) is U magnitude per square of arcseconds. The brightness is normalized by the magnitude SB_0 at the smallest radius point. In the legend, '(c)' means PCC cluster as judged so in (Djorgovski and King, 1986). $\Delta(SB_0 - SB)$ is the corresponding deviation of $SB_0 - SB$ from the model.

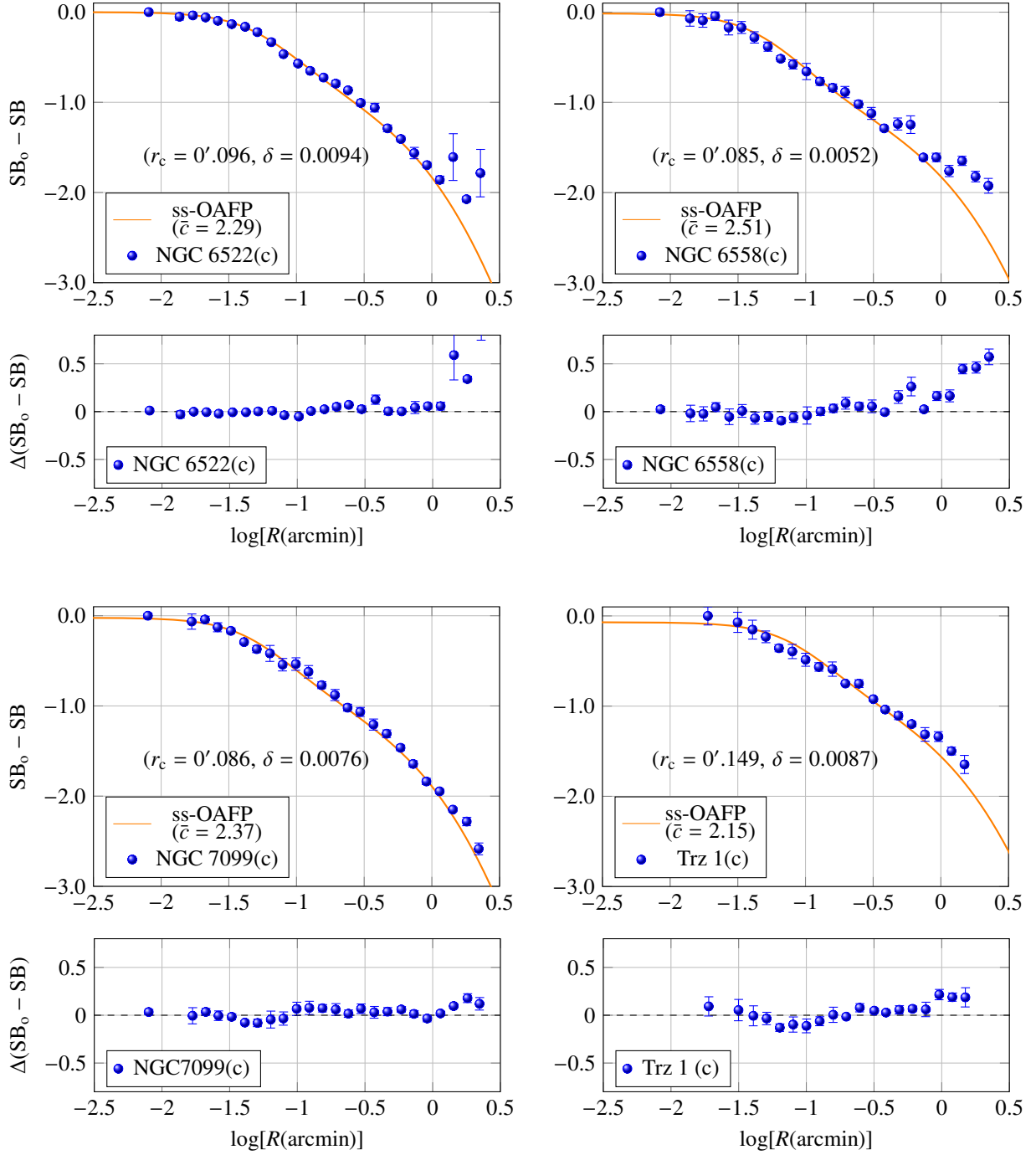


Figure B.31: Fitting of the energy-truncated ss-OAFP model to the surface brightness profiles of NGC 6522, NGC 6558 and NGC 7099 reported in (Lugger et al., 1995) and Terzan 1 reported in (Djorgovski and King, 1986). The unit of the surface brightness (SB) is U magnitude per square of arcseconds except for Terzan 1 for which B band is used. The brightness is normalized by the magnitude SB_0 at the smallest radius point. In the legend, '(c)' means PCC cluster as judged so in (Djorgovski and King, 1986). $\Delta(SB_0 - SB)$ is the corresponding deviation of $SB_0 - SB$ from the model.

B.3 PCC clusters (Noyola and Gebhardt, 2006)

The energy-truncated ss-OAFP model with $m = 4.2$ well fits the surface brightness profiles of PCC clusters reported in (Noyola and Gebhardt, 2006) as shown in Figure B.32. However, NGC 6624 is an example of failure of our model as shown in Figure B.33. This failure also occurred to the same cluster but reported in (Lugger et al., 1995) (Appendix B.2). It appears that NGC 6624 needs more realistic effects, such as the binary heating and mass function. Also, NGC 6541 has also a cusp in the core that our model can not fit.

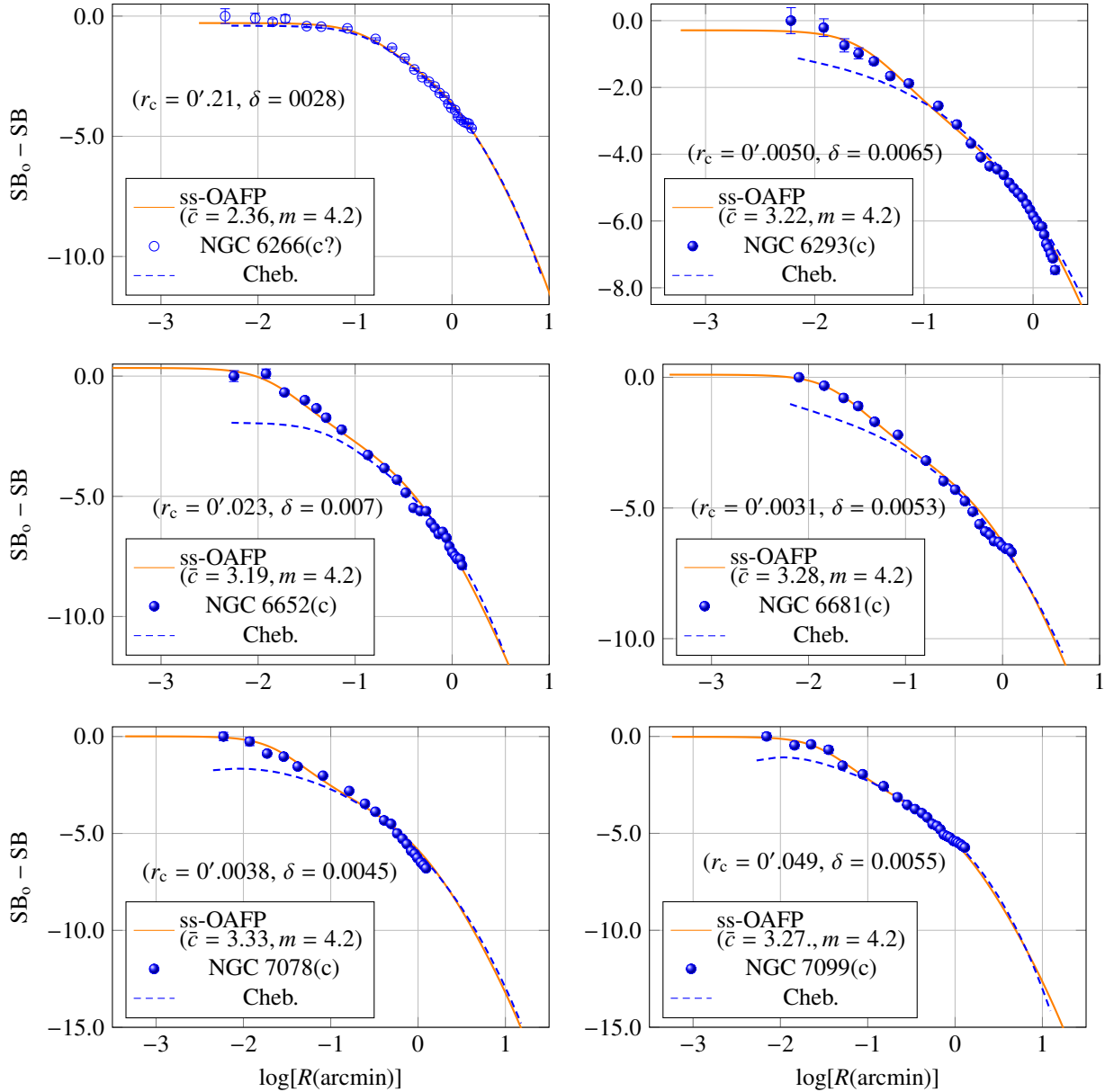


Figure B.32: Fitting of the energy-truncated ss-OAFP model to the surface brightness profiles of NGC 6266, NGC 6293, NGC 6652, NGC 6681, NGC 7078 and NGC 7099 reported in (Noyola and Gebhardt, 2006). The unit of the surface brightness (SB) is V magnitude per square of arcseconds. The brightness is normalized by the magnitude SB_0 at the smallest radius point. In the legend, ‘Cheb.’ means the Chebyshev approximation of the surface brightness profiles reported in (Trager et al., 1995) and ‘(c)’ means PCC cluster as judged so in (Djorgovski and King, 1986). $\Delta(SB_0 - SB)$ is the corresponding deviation of $SB_0 - SB$ from the model

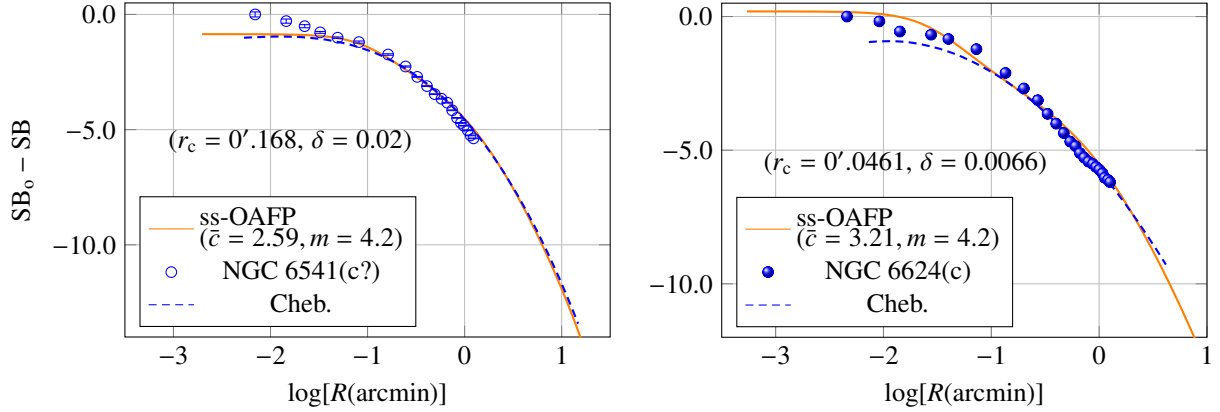


Figure B.33: Failure of fitting of the energy-truncated ss-OAFP model to the surface brightness profiles of NGC 6541 and NGC 6624 reported in (Noyola and Gebhardt, 2006). The unit of the surface brightness (SB) is V magnitude per square of arcseconds. The brightness is normalized by the magnitude SB_0 at the smallest radius point. In the legend, ‘Cheb.’ means the Chebyshev approximation of the surface brightness profiles reported in (Trager et al., 1995) and ‘(c)’ means PCC cluster and ‘(c?)’ possibly PCC cluster as judged so in (Djorgovski and King, 1986). $\Delta(SB_0 - SB)$ is the corresponding deviation of $SB_0 - SB$ from the model

Appendix C Fitting of the finite ss-OAFP model to Post-collapsed-core clusters

The present Appendix shows the fitting of polytropic sphere of index m to the projected density profiles and surface brightness of low-concentration globular clusters reported in (Miocchi et al., 2013; Trager et al., 1995; Kron et al., 1984). Fitting of the polytrope is done for (Miocchi et al., 2013)’s data by minimizing χ^2_ν and for (Kron et al., 1984; Trager et al., 1995)’s data by minimizing the infinite norm of residues for the differences between the fitted curve and the data.

C.1 Polytropic cluster (Miocchi et al., 2013) and (Kron et al., 1984)

Figures C.34 and C.35 show successful application of the polytrope model to the projected density profiles of NGC 5466, NGC 6809, Palomar 3, Palomar 4 and Palomar 14 reported in (Miocchi et al., 2013). In the figures, the polytropes of $3.0 < m < 5$ reasonably fit to the projected surface densities of the globular clusters whose concentrations range $1 < \bar{c} < 1.4$. Figure C.36 shows the projected density of NGC 4590 fitted with a polytrope. NGC 4590 is one of the examples that could fall in either of polytropic and non-polytropic .

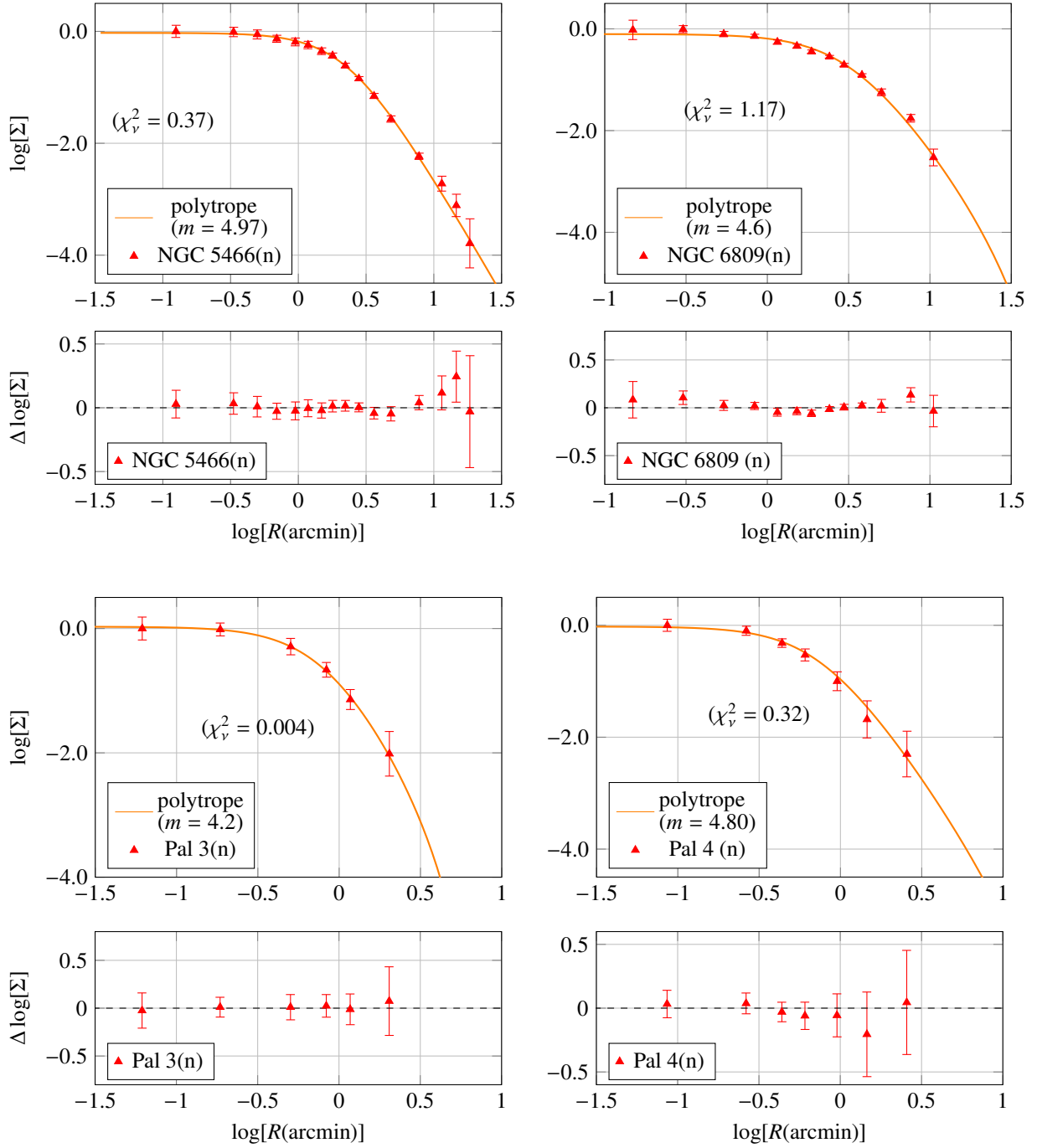


Figure C.34: Fitting of the polytropic sphere of index m to the projected density Σ of NGC 5466, NGC 6809, Palomar 3 and Palomar 4 reported in (Miocchi et al., 2013). The unit of Σ is number per square of arcminutes and Σ is normalized so that the density is unity at smallest radius for data. In the legends, (n) means normal or KM cluster as judged so in (Djorgovski and King, 1986). $\Delta \log[\Sigma]$ is the corresponding deviation of Σ from the model on log scale.

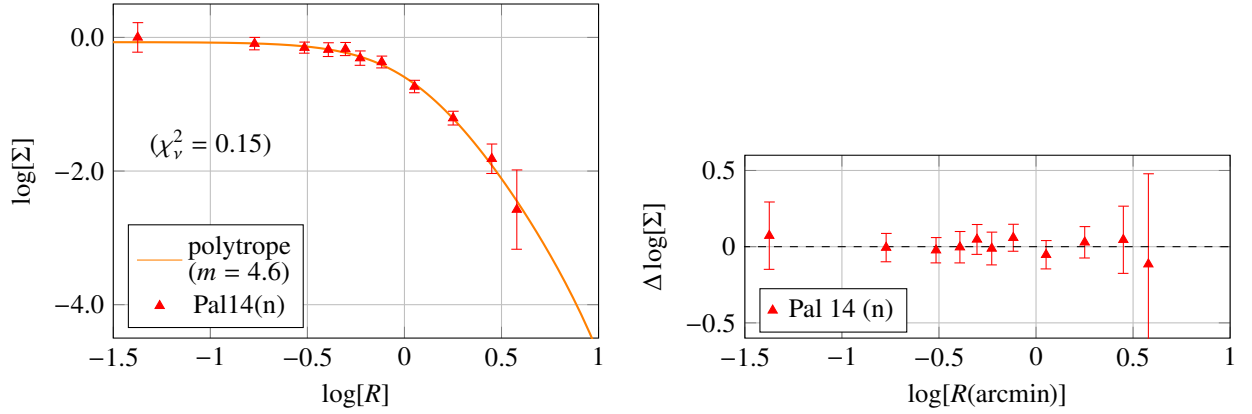


Figure C.35: Fitting of the polytropic sphere of index m to the projected density of Palomar 14 reported in (Miocchi et al., 2013). The unit of the projected density Σ is number per square of arcminutes. In the legends, (n) means normal or KM cluster as judged so in (Djorgovski and King, 1986).

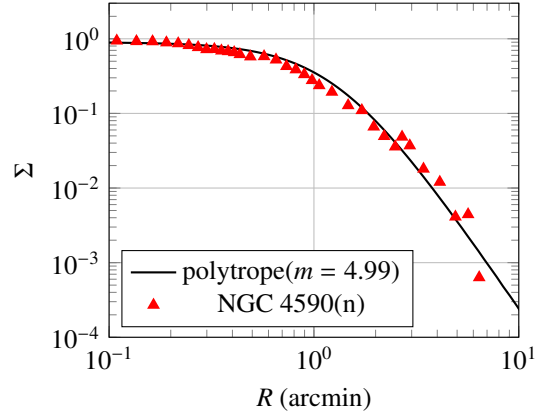


Figure C.36: Partial success of fitting of the polytropic sphere of index m to the projected density of NGC 4590 reported in (Kron et al., 1984). The unit of the projected density Σ is number per square of arcminutes. In the legends, (n) means normal or KM cluster as judged so in (Djorgovski and King, 1986). Following (Kron et al., 1984), data at small radii are ignored due to the depletion of projected density profile.

C.2 Polytropic cluster (Trager et al., 1995)

Figures C.37 and C.38 depict the fitting of the polytropic sphere model to the Chebyshev approximation to the surface brightness profiles reported in (Trager et al., 1995). The polytropic indices $m = 3.3 \sim 4.99$ are useful to fit the polytropic model to the low-concentration clusters whose core relaxation time are order of 1 Gyr (from (Harris, 1996, (2010 edition))'s catalog). Since the polytrope itself does not rapidly decay near its limiting radius, the corresponding concentrations of the polytrope are relatively high such as $\bar{c} = 3.34$ for $m = 4.99$. On one hand, Figure C.39 shows the clusters whose surface brightness profiles are not close to the polytrope. Such clusters have shorter core relaxation times < 0.5 Gyr and relatively high concentrations $c > 1.5$ (based on the King model) as shown in Table 3.

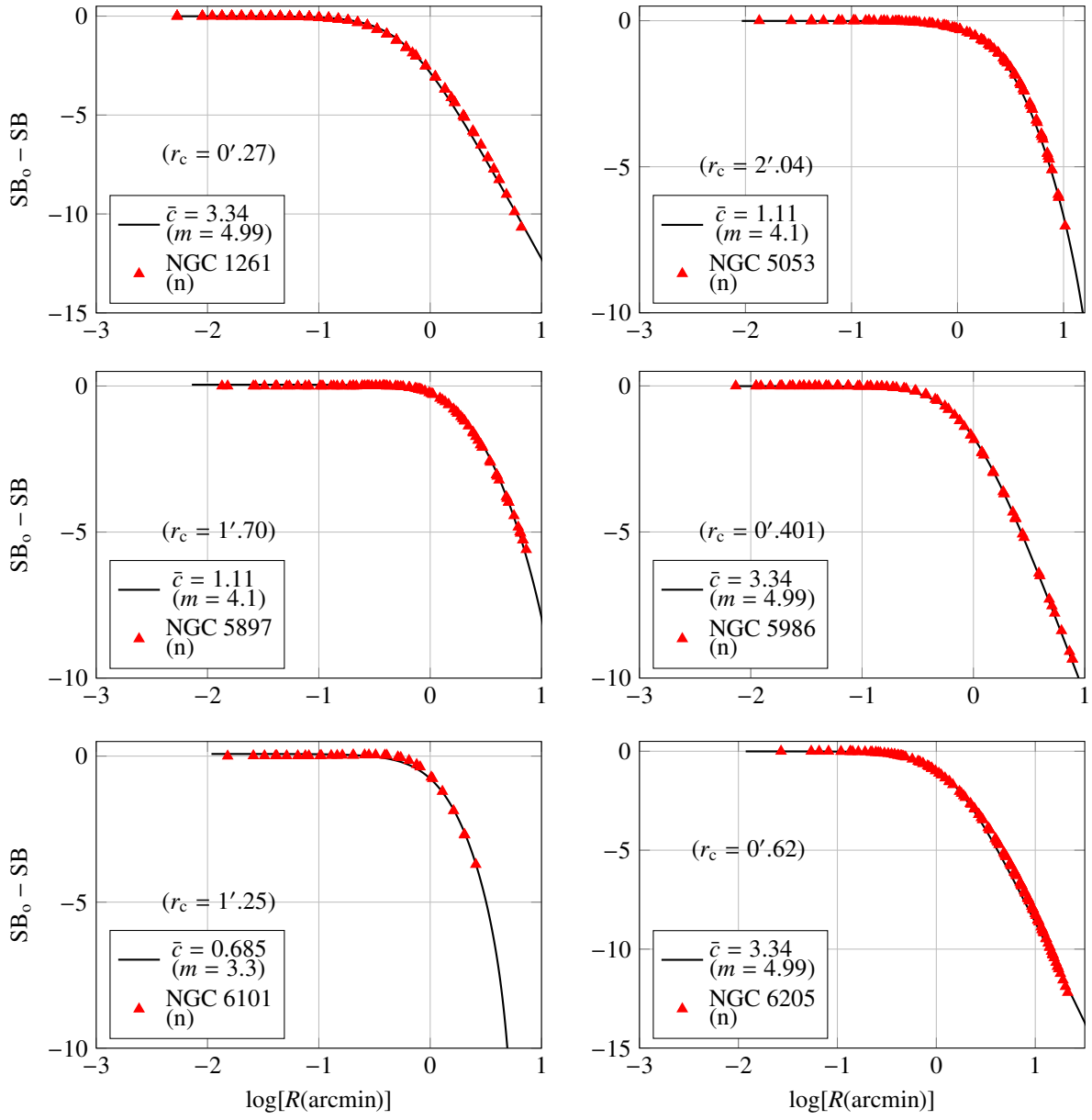


Figure C.37: Fitting of the polytropic sphere of index m to the surface brightness profiles of NGC 1261, NGC 5053, NGC 5897, NGC 5986, NGC 6101 and NGC 6205 reported in Trager et al. (1995). The unit of the surface brightness (SB) is V magnitude per square of arcseconds. The brightness is normalized by the magnitude SB_0 at the smallest radius point. In the legends, '(n)' means KM cluster as judged so in (Djorgovski and King, 1986).

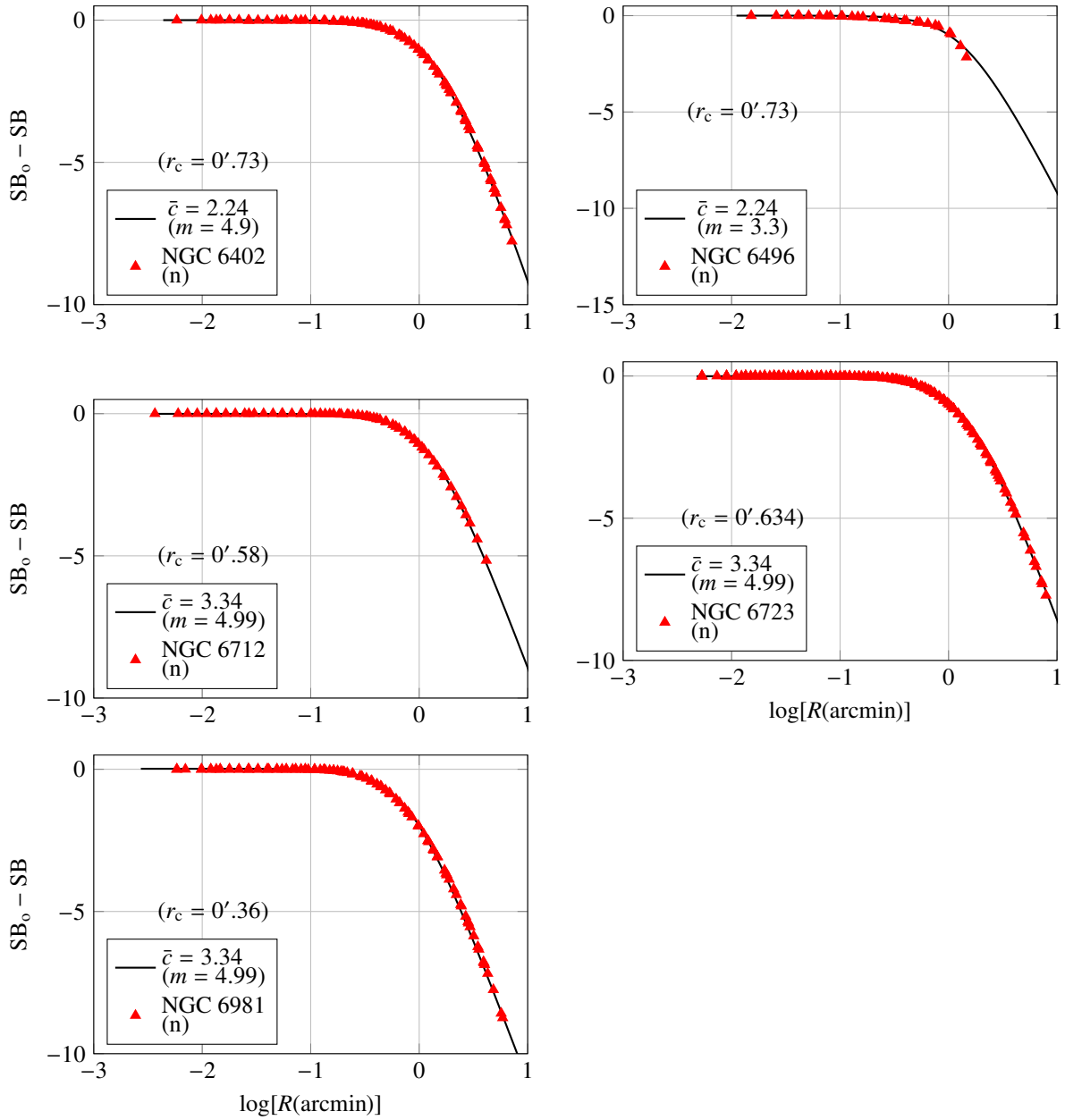


Figure C.38: Fitting of the polytropic sphere of index m to the surface brightness profiles of NGC 6402, NGC 6496, NGC 6712, NGC 6723 and NGC 6981 reported in (Trager et al., 1995). The unit of the surface brightness (SB) is V magnitude per square of arcseconds. The brightness is normalized by the magnitude SB_0 at the smallest radius point. In the legends, '(n)' means KM cluster as judged so in (Djorgovski and King, 1986).

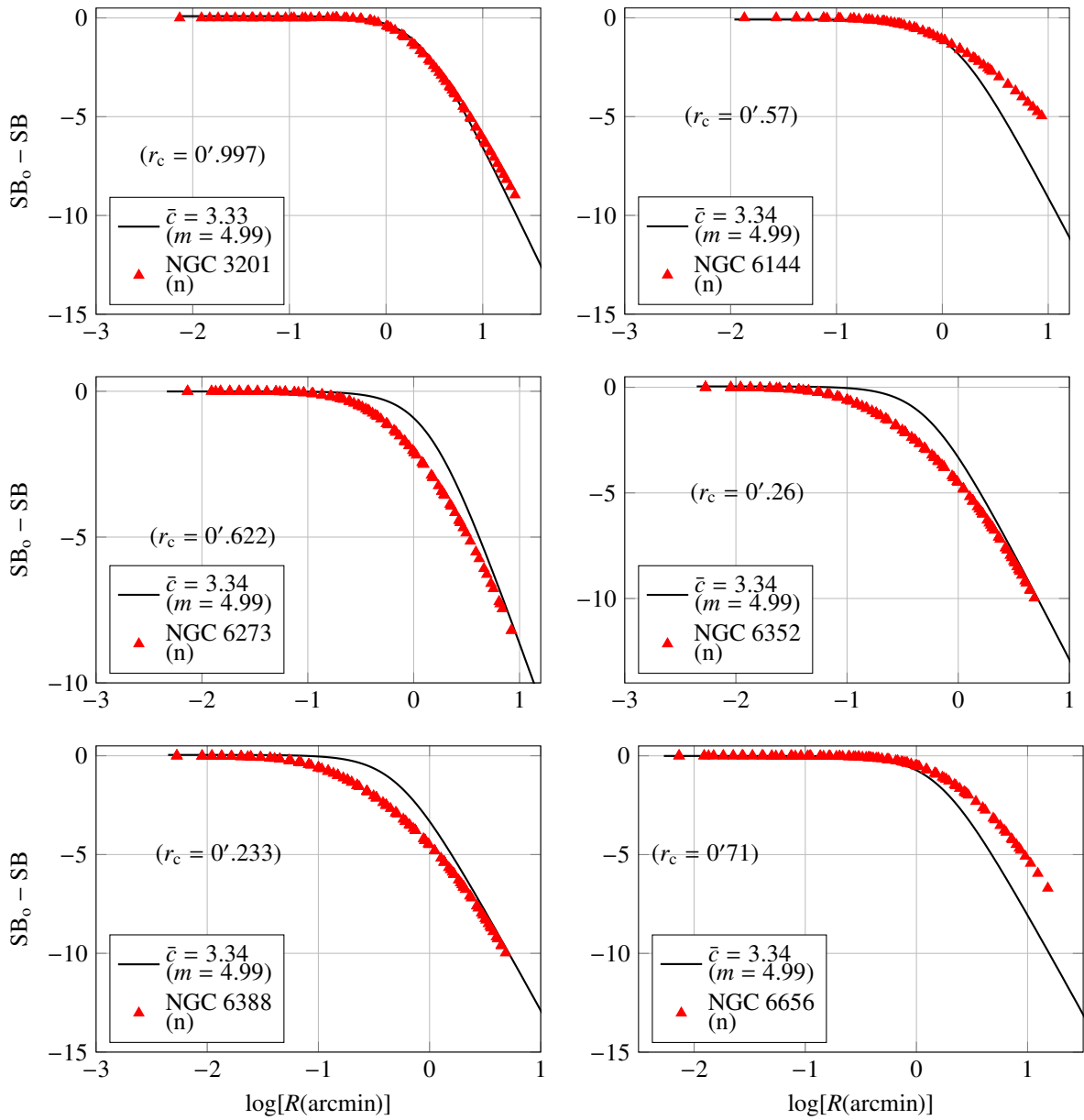


Figure C.39: Failure of fitting of the polytropic sphere of index m to the surface brightness profiles of NGC 3201, NGC 6144, NGC 6273, NGC 6352, NGC 6388 and NGC 6656 reported in (Trager et al., 1995). The unit of the surface brightness (SB) is V magnitude per square of arcseconds. The brightness is normalized by the magnitude SB_0 at the smallest radius point. In the legends, '(n)' means KM cluster as judged so in (Djorgovski and King, 1986).

Aarseth, S. J., Heggie, D. C., 1998. Basic n-body modelling of the evolution of globular clusters — i. time scaling. *Monthly Notices of the Royal Astronomical Society* 297 (3), 794–806.
 URL <http://dx.doi.org/10.1046/j.1365-8711.1998.01521.x>

Baumgardt, H., Hilker, M., Sollima, A., Bellini, A., nov 2018. Mean proper motions, space orbits, and velocity dispersion profiles of galactic globular clusters derived from GaiaDR2 data. *Monthly Notices of the Royal Astronomical Society* 482 (4), 5138–5155.
 URL <https://doi.org/10.1093/mnras/sty2997>

Baumgardt, H., Hut, P., Heggie, D. C., nov 2002. Long-term evolution of isolated n-body systems. *Monthly Notices of the Royal Astronomical Society* 336 (4), 1069–1081.
 URL <https://doi.org/10.1046/j.1365-8711.2002.05736.x>

Baumgardt, H., Makino, J., mar 2003. Dynamical evolution of star clusters in tidal fields. *Monthly Notices of the Royal Astronomical Society*

- 340 (1), 227–246.
 URL <https://doi.org/10.1046%2Fj.1365-8711.2003.06286.x>
- Baumgardt, H., Marchi, G. D., Kroupa, P., sep 2008. Evidence for primordial mass segregation in globular clusters. *The Astrophysical Journal* 685 (1), 247–253.
 URL <https://doi.org/10.1086%2F590488>
- Bettwieser, E., Sugimoto, D., jun 1984. Post-collapse evolution and gravothermal oscillation of globular clusters. *Monthly Notices of the Royal Astronomical Society*.
 URL <https://doi.org/10.1093%2Fmnras%2F208.3.493>
- Binney, J., Tremaine, S., 2011. *Galactic Dynamics*. Princeton university press.
- Boyd, J. P., jun 2011. Chebyshev spectral methods and the lane-Emden problem. *Numerical Mathematics: Theory, Methods and Applications* 4 (2), 142–157.
 URL <https://doi.org/10.4208%2Fnmmta.2011.42s.2>
- Breen, P. G., Heggie, D. C., aug 2012. Gravothermal oscillations in multicomponent models of star clusters. *Monthly Notices of the Royal Astronomical Society* 425 (4), 2493–2500.
 URL <https://doi.org/10.1111%2Fj.1365-2966.2012.21688.x>
- Chandrasekhar, S., 1939. An introduction to the study of stellar structure. Chicago, Ill., The University of Chicago press.
- Chandrasekhar, S., Jan 1943. Stochastic Problems in Physics and Astronomy. *Rev. Mod. Phys.* 15, 1–89.
 URL <https://link.aps.org/doi/10.1103/RevModPhys.15.1>
- Chernoff, D. F., Djorgovski, S., apr 1989. An analysis of the distribution of globular clusters with postcollapse cores in the galaxy. *The Astrophysical Journal* 339, 904.
 URL <https://doi.org/10.1086%2F167344>
- Chernoff, D. F., Weinberg, M. D., mar 1990. Evolution of globular clusters in the galaxy. *The Astrophysical Journal* 351, 121.
 URL <https://doi.org/10.1086%2F168451>
- Claydon, I., Gieles, M., Varri, A. L., Heggie, D. C., Zocchi, A., may 2019. Spherical models of star clusters with potential escapers. *Monthly Notices of the Royal Astronomical Society* 487 (1), 147–160.
 URL <https://doi.org/10.1093%2Fmnras%2Fstz1109>
- Cohn, H., dec 1980. Late core collapse in star clusters and the gravothermal instability. *The Astrophysical Journal* 242, 765.
 URL <https://doi.org/10.1086%2F158511>
- Cohn, H., Hut, P., Wise, M., jul 1989. Gravothermal oscillations after core collapse in globular cluster evolution. *The Astrophysical Journal* 342, 814.
 URL <https://doi.org/10.1086%2F167638>
- de Boer, T. J. L., Gieles, M., Balbinot, E., Hénault-Brunet, V., Sollima, A., Watkins, L. L., Claydon, I., mar 2019. Globular cluster number density profiles using Gaia DR2. *Monthly Notices of the Royal Astronomical Society* 485 (4), 4906–4935.
 URL <https://doi.org/10.1093%2Fmnras%2Fstz651>
- de Vita, R., Bertin, G., Zocchi, A., apr 2016. A class of spherical, truncated, anisotropic models for application to globular clusters. *Astronomy & Astrophysics* 590, A16.
 URL <https://doi.org/10.1051%2F0004-6361%2F201628274>
- Djorgovski, S., King, I. R., jun 1986. A preliminary survey of collapsed cores in globular clusters. *The Astrophysical Journal* 305, L61.
 URL <https://doi.org/10.1086%2F184685>
- Dotter, A., Sarajedini, A., Anderson, J., Aparicio, A., Bedin, L. R., Chaboyer, B., Majewski, S., Marín-Franch, A., Milone, A., Paust, N., Piotto, G., Reid, I. N., Rosenberg, A., Siegel, M., dec 2009. THE ACS SURVEY OF GALACTIC GLOBULAR CLUSTERS. IX. HORIZONTAL BRANCH MORPHOLOGY AND THE SECOND PARAMETER PHENOMENON. *The Astrophysical Journal* 708 (1), 698–716.
 URL <https://doi.org/10.1088%2F0004-637x%2F708%2F1%2F698>
- Drukier, G., Fahlman, G., Richer, H., Searle, L., Thompson, I., 1993. Star counts in NGC 6397. arXiv preprint astro-ph/9309005.
- Drukier, G. A., oct 1995. Fokker-planck models of NGC 6397. *The Astrophysical Journal Supplement Series* 100, 347.
 URL <https://doi.org/10.1086%2F192223>
- Drukier, G. A., Fahlman, G. G., Richer, H. B., feb 1992. Fokker-planck models and globular cluster evolution - the problem of M71. *The Astrophysical Journal* 386, 106.
 URL <https://doi.org/10.1086%2F170997>
- Ferraro, F. R., Mucciarelli, A., Lanzoni, B., Pallanca, C., Lapenna, E., Origlia, L., Dalessandro, E., Valenti, E., Beccari, G., Bellazzini, M., Vesperini, E., Varri, A., Sollima, A., jun 2018. MIKIS: The multi-instrument kinematic survey of galactic globular clusters. I. Velocity dispersion profiles and rotation signals of 11 globular clusters. *The Astrophysical Journal* 860 (1), 50.
 URL <https://doi.org/10.3847%2F1538-4357%2Faabe2f>
- Ferraro, F. R., Possenti, A., Sabbi, E., Lagani, P., Rood, R. T., D’Amico, N., Origlia, L., sep 2003. The puzzling dynamical status of the core of the globular cluster NGC 6752. *The Astrophysical Journal* 595 (1), 179–186.
 URL <https://doi.org/10.1086%2F377352>
- Forbes, D. A., Bridges, T., feb 2010. Accreted versus in situ Milky Way globular clusters. *Monthly Notices of the Royal Astronomical Society*.
 URL <https://doi.org/10.1111%2Fj.1365-2966.2010.16373.x>
- Fukushige, T., Heggie, D. C., 1996. Pre-collapse evolution of galactic globular clusters. *Symposium - International Astronomical Union* 174, 365–366.
 URL <https://doi.org/10.1017%2Fs0074180900001844>
- Gieles, M., Zocchi, A., sep 2015. A family of lowered isothermal models. *Monthly Notices of the Royal Astronomical Society* 454 (1), 576–592.
 URL <https://doi.org/10.1093%2Fmnras%2Fstv1848>
- Gomez-Leyton, Y. J., Velazquez, L., apr 2014. Truncated γ -exponential models for tidal stellar systems. *Journal of Statistical Mechanics: Theory and Experiment* 2014 (4), P04006.

- URL <https://doi.org/10.1088%2F1742-5468%2F2014%2F04%2Fp04006>
- Goodman, J., may 1984. Homologous evolution of stellar systems after core collapse. *The Astrophysical Journal* 280, 298.
URL <https://doi.org/10.1086%2F161996>
- Goodman, J., feb 1987. On gravothermal oscillations. *The Astrophysical Journal* 313, 576.
URL <https://doi.org/10.1086%2F164998>
- Goodman, J., Hut, P., may 1989. Primordial binaries and globular cluster evolution. *Nature* 339 (6219), 40–42.
URL <https://doi.org/10.1038%2F339040a0>
- Harris, W. E., oct 1996. A catalog of parameters for globular clusters in the milky way. *The Astronomical Journal* 112, 1487.
URL <https://doi.org/10.1086%2F118116>
- Inagaki, S., Lynden-Bell, D., dec 1983. Self-similar solutions for post-collapse evolution of globular clusters. *Monthly Notices of the Royal Astronomical Society* 205 (4), 913–930.
URL <https://doi.org/10.1093%2Fmnras%2F205.4.913>
- Ito, Y., Aug 2018. An orbit-averaged generalised-Landau-kinetic equation for probability distribution of N -stars in finite dense weakly-coupled star clusters. arXiv e-prints, arXiv:1808.09895.
- Ito, Y., Mar. 2020a. Self-similar orbit-averaged Fokker-Planck equation for isotropic spherical dense clusters (i) accurate pre-collapse solution. arXiv e-prints, arXiv:2003.12196.
- Ito, Y., Mar. 2020b. Self-similar orbit-averaged Fokker-Planck equation for isotropic spherical dense clusters (ii) Physical properties and negative heat capacity of pre-collapse core. arXiv e-prints, arXiv:2003.13179.
- Ito, Y., Poje, A., Lancellotti, C., jan 2018. Very-large-scale spectral solutions for spherical polytropes of index $m \lesssim 5$ and the isothermal sphere. *New Astronomy* 58, 15–28.
URL <https://doi.org/10.1016%2Fj.newast.2017.07.003>
- Kandrup, H., feb 1981. Generalized landau equation for a system with a self-consistent mean field - derivation from an n-particle liouville equation. *The Astrophysical Journal* 244, 316.
URL <https://doi.org/10.1086%2F158709>
- Kandrup, H. E., 1985. Should a self-gravitating system relax towards an isothermal distribution? *Astrophysics and Space Science* 112 (2), 215–223.
URL <https://doi.org/10.1007%2Fb00653505>
- Kandrup, H. E., 1988. 'discreteness fluctuations' and relaxation in stellar dynamical systems. *Monthly Notices of the Royal Astronomical Society* 235 (4), 1157.
URL <http://dx.doi.org/10.1093/mnras/235.4.1157>
- Kerber, L. O., Nardiello, D., Ortolani, S., Barbuy, B., Bica, E., Cassisi, S., Libralato, M., Vieira, R. G., jan 2018. Ages of the bulge globular clusters NGC 6522 and NGC 6626 (m28) from HST Proper-motion-cleaned color–magnitude diagrams. *The Astrophysical Journal* 853 (1), 15.
URL <https://doi.org/10.3847%2F1538-4357%2Faaa3fc>
- King, I. R., jun 1965. The structure of star clusters. II. steady-state velocity distributions. *The Astronomical Journal* 70, 376.
URL <https://doi.org/10.1086%2F109750>
- King, I. R., feb 1966. The structure of star clusters. III. some simple dynamical models. *The Astronomical Journal* 71, 64.
URL <https://doi.org/10.1086%2F109857>
- King, I. R., Sosin, C., Cool, A. M., oct 1995. Mass segregation in the globular cluster NGC 6397. *The Astrophysical Journal* 452 (1).
URL <https://doi.org/10.1086%2F309703>
- Kron, G. E., Hewitt, A. V., Wasserman, L. H., mar 1984. Brightness profiles for 69 globular clusters determined by means of the electronic camera. *Publications of the Astronomical Society of the Pacific* 96, 198.
URL <https://doi.org/10.1086%2F131322>
- Lightman, A. P., dec 1982. What has happened in the cores of globular clusters. *The Astrophysical Journal* 263, L19.
URL <https://doi.org/10.1086%2F183915>
- Lugger, P. M., Cohn, H. N., Grindlay, J. E., jan 1995. CCD photometry of globular cluster core structure. 2: U-band profiles for 15 candidate collapsed-core clusters. *The Astrophysical Journal* 439, 191.
URL <https://doi.org/10.1086%2F175164>
- Makino, J., nov 1996. Postcollapse evolution of globular clusters. *The Astrophysical Journal* 471 (2), 796–803.
URL <https://doi.org/10.1086%2F178007>
- Mandushev, G., Staneva, A., Spasova, N., Dec 1991. Dynamical masses for galactic globular clusters. *aap* 252, 94.
- Marchi, G. D., Paresce, F., Pulone, L., jan 2007. Why haven't loose globular clusters collapsed yet? *The Astrophysical Journal* 656 (2), L65–L68.
URL <https://doi.org/10.1086%2F512856>
- Merafina, M., apr 2017. Dynamical evolution of globular clusters: Recent developments. *International Journal of Modern Physics D* 26 (09), 1730017.
URL <https://doi.org/10.1142%2Fs0218271817300178>
- Meylan, G., 1987. Studies of dynamical properties of globular clusters. iii-anisotropy in omega centauri. *Astronomy and Astrophysics* 184, 144–154.
- Meylan, G., Heggie, D., feb 1997. Internal dynamics of globular clusters. *Astronomy and Astrophysics Review* 8 (1-2), 1–143.
URL <https://doi.org/10.1007%2Fs001590050008>
- Michie, R. W., aug 1962. On the distribution of high energy stars in spherical stellar systems. *Monthly Notices of the Royal Astronomical Society* 125 (2), 127–139.
URL <https://doi.org/10.1093%2Fmnras%2F125.2.127>
- Miocchi, P., Lanzoni, B., Ferraro, F. R., Dalessandro, E., Vesperini, E., Pasquato, M., Beccari, G., Pallanca, C., Sanna, N., aug 2013. STAR COUNT DENSITY PROFILES AND STRUCTURAL PARAMETERS OF 26 GALACTIC GLOBULAR CLUSTERS. *The Astrophysical Journal* 774 (2), 151.
URL <https://doi.org/10.1088%2F0004-637x%2F774%2F2%2F151>

- Murphy, B. W., Cohn, H. N., Hut, P., Jul 1990. Realistic models for evolving globular clusters - II. POST core collapse with a mass spectrum. *mnras* 245, 335.
- Murphy, B. W., Cohn, H. N., Lugger, P. M., apr 2011. FOKKER-PLANCK MODELS FOR m15 WITHOUT a CENTRAL BLACK HOLE: THE ROLE OF THE MASS FUNCTION. *The Astrophysical Journal* 732 (2), 67.
URL <https://doi.org/10.1088%2F0004-637x%2F732%2F2%2F67>
- Noyola, E., Gebhardt, K., jun 2006. Surface brightness profiles of galactic globular clusters from Hubble space Telescope Images. *The Astronomical Journal* 132 (2), 447–466.
URL <https://doi.org/10.1086%2F505390>
- Peterson, C. J., King, I. R., jun 1975. The structure of stars. VI. observed radii and structural parameters in globular clusters. *The Astronomical Journal* 80, 427.
URL <https://doi.org/10.1086%2F111759>
- Polyachenko, V. L., Shukhman, I. G., Apr. 1982. Collisions in Spherical Stellar Systems. *Soviet Astronomy* 26, 140–145.
- Portegies Zwart, S. F., Hut, P., Makino, J., McMillan, S. L. W., Sep 1998. On the dissolution of evolving star clusters. *aap* 337, 363–371.
- Rohatgi, A., Apr 2019. Webplotdigitizer (version 4.2) Available at <https://automeris.io/WebPlotDigitizer>.
URL <https://automeris.io/WebPlotDigitizer>
- Salaris, M., Weiss, A., may 2002. Homogeneous age dating of 55 galactic globular clusters. *Astronomy & Astrophysics* 388 (2), 492–503.
URL <https://doi.org/10.1051%2F0004-6361%3A20020554>
- Santos, J. F. C., Piatti, A. E., nov 2004. Ages and metallicities of star clusters: New calibrations and diagnostic diagrams from visible integrated spectra. *Astronomy & Astrophysics* 428 (1), 79–88.
URL <https://doi.org/10.1051%2F0004-6361%3A20041560>
- Sollima, A., Martínez-Delgado, D., Valls-Gabaud, D., Peñarrubia, J., dec 2010. DISCOVERY OF TIDAL TAILS AROUND THE DISTANT GLOBULAR CLUSTER PALOMAR 14. *The Astrophysical Journal* 726 (1), 47.
URL <https://doi.org/10.1088%2F0004-637x%2F726%2F1%2F47>
- Spitzer, L. J., Harm, R., may 1958. Evaporation of stars from isolated clusters. *The Astrophysical Journal* 127, 544.
URL <https://doi.org/10.1086%2F146486>
- Spitzer, L. J., Shapiro, S. L., may 1972. Random gravitational encounters and the evolution of spherical systems. III. halo. *The Astrophysical Journal* 173, 529.
URL <https://doi.org/10.1086%2F151442>
- Spitzer, L. S., jan 1988. Dynamical Evolution of Globular Clusters. Walter de Gruyter GmbH.
URL <http://dx.doi.org/10.1515/9781400858736>
- Sugimoto, D., Bettwieser, E., sep 1983. Post-collapse evolution of globular clusters. *Monthly Notices of the Royal Astronomical Society* 204 (1), 19P–22P.
URL <https://doi.org/10.1093%2Fmnras%2F204.1.19p>
- Takahashi, K., oct 1996. Fokker-planck models of star clusters with anisotropic velocity distributions II. post-collapse evolution. *Publications of the Astronomical Society of Japan* 48 (5), 691–700.
URL <https://doi.org/10.1093%2Fpasj%2F48.5.691>
- Takahashi, K., Lee, H. M., aug 2000. Evolution of multimass globular clusters in the galactic tidal field with the effects of velocity anisotropy. *Monthly Notices of the Royal Astronomical Society* 316 (3), 671–683.
URL <https://doi.org/10.1046%2Fj.1365-8711.2000.03594.x>
- Taruya, A., Sakagami, M., may 2003. Long-term evolution of stellar self-gravitating systems away from thermal equilibrium: connection with nonextensive statistics. *Phys. Rev. Lett.* 90 (18).
URL <http://dx.doi.org/10.1103/physrevlett.90.181101>
- Taruya, A., Sakagami, M., sep 2004. Fokker–Planck study of stellar self-gravitating system away from the thermal equilibrium: connection with non-extensive statistics. *Physica A: Statistical Mechanics and its Applications* 340 (1-3), 453–458.
URL <http://dx.doi.org/10.1016/j.physa.2004.04.040>
- Trager, S., Djorgovski, S., King, I., 1993. Structural Parameters of Galactic Globular Clusters. Vol. 50 of *Astronomical Society of the Pacific Conference Series*. Astronomical Society of the Pacific, p. 347.
- Trager, S. C., King, I. R., Djorgovski, S., jan 1995. Catalogue of galactic globular-cluster surface-brightness profiles. *The Astronomical Journal* 109, 218.
URL <https://doi.org/10.1086%2F117268>
- Wang, L., Spurzem, R., Aarseth, S., Giersz, M., Askar, A., Berczik, P., Naab, T., Schadow, R., Kouwenhoven, M. B. N., feb 2016. The dragon simulations: globular cluster evolution with a million stars. *Monthly Notices of the Royal Astronomical Society* 458 (2), 1450–1465.
URL <https://doi.org/10.1093%2Fmnras%2F458.2.1450>
- Wilson, C. P., mar 1975. Dynamical models of elliptical galaxies. *The Astronomical Journal* 80, 175.
URL <https://doi.org/10.1086%2F111729>
- Woolley, R., Oct 1961. Globular clusters. *The Observatory* 81, 161–182.
- Zonoozi, A. H., Hagh, H., Kroupa, P., Küpper, A. H., Baumgardt, H., jan 2017. Direct n-body simulations of globular clusters – III. palomar 4 on an eccentric orbit. *Monthly Notices of the Royal Astronomical Society*, stx130.
URL <https://doi.org/10.1093%2Fmnras%2Fstx130>